

Gaining Insights on the Interactions of a Class of Decorated (2-([2,2'-Bipyridin]-6-yl)phenyl)platinum Compounds with c-Myc Oncogene Promoter G-Quadruplex and Other DNA Structures

Loukiani Savva,^[a] Mathieu Fossépré,^[b] Odysseas Keramidas,^[a] Alexandros Themistokleous,^[a] Natalia Rizeq,^[a] Nikos Panagiotou,^[a] Maxime Leclercq,^[b] Eliana Nicolaidou,^[a] Mathieu Surin,^{*,[b]} Sophia C. Hayes,^[a] and Savvas N. Georgiades^{*,[a]}

Abstract: Organometallic molecules offer some of the most promising scaffolds for interaction with G-quadruplex nucleic acids. We report the efficient synthesis of a family of organoplatinum(II) complexes, featuring a 2-([2,2'-bipyridin]-6-yl)phenyl tridentate (N^NC) ligand, that incorporates peripheral side-chains aiming at enhancing and diversifying its interaction capabilities. These include a di-isopropyl carbamoyl amide, a morpholine ethylenamide, two enantiomeric proline imides and an oxazole. The binding affinities of the Pt-complexes were evaluated via UV-vis and fluorescence titrations, against 5 topologically-distinct DNA structures, including c-myc G-quadruplex, two telomeric (22AG) G-quadruplexes, a duplex (ds26) and a single-stranded (polyT) DNA. All compounds exhibited binding selectivity in favour of c-myc, with association constants (K_a) in the range of $2\text{--}5 \times 10^5 \text{ M}^{-1}$, lower affinity for both folds of 22AG and for ds26 and negligible affinity for polyT. Remarkable emission enhancements (up to 200-fold) upon addition of excess DNA were demonstrated by a subset of the compounds with c-

myc, providing a basis for optical selectivity, since optical response to all other tested DNAs was low. A c-myc DNA-melting experiment showed significant stabilizing abilities for all compounds, with the most potent binder, the morpholine-Pt-complex, exhibiting a $\Delta T_m > 30^\circ\text{C}$, at 1:5 DNA-to-ligand molar ratio. The same study implied contributions of the diverse side-chains to helix stabilization. To gain direct evidence of the nature of the interactions, mixtures of c-myc with the four most promising compounds were studied via UV Resonance Raman (UVRM) spectroscopy, which revealed end-stacking binding mode, combined with interactions of side-chains with loop nucleobase residues. Docking simulations were conducted to provide insights into the binding modes for the same four Pt-compounds, suggesting that the binding preference for two alternative orientations of the c-myc G-quadruplex thymine 'cap' ('open' vs. 'closed'), as well as the relative contributions to affinity from end-stacking and H-bonding, are highly dependent on the nature of the interacting Pt-complex side-chain.

Introduction

Over the last decade, the family of non-canonical nucleic acid topologies known as G-quadruplexes have become the object of a vast number of studies, owing to their emerging biological roles, including telomerase inhibition,^[1] involvement in chromatin remodelling,^[2] epigenetic alteration^[3] and genome instability,^[4] as well as regulation of replication,^[5] transcription^[6] and translation.^[7]

G-quadruplexes are tetraplex helices, assembled from guanine (G)-rich DNA or RNA sequences, in which the presence of repetitive guanine tracts enables formation of square planar G-quartets via Hoogsteen-face hydrogen bonding. G-quartets are further reinforced by guanine carbonyl coordination to (monovalent) cations. G-quartet $\pi\text{--}\pi$ stacking-type accumulation is responsible for the G-quadruplex core assembly.^[8] Extensive polymorphism is observed among G-quadruplexes, depending on the environmental conditions, and associated with different orientations of the four contributing strands, as well as the type, length and sequence of their interconnecting loops.^[9]

[a] L. Savva, O. Keramidas, A. Themistokleous, N. Rizeq, Dr. N. Panagiotou, E. Nicolaidou, Dr. S. C. Hayes, Dr. S. N. Georgiades
Department of Chemistry
University of Cyprus
1 Panepistimiou Avenue, Aglandjia, 2109 Nicosia (Cyprus)
E-mail: georgiades.savvas@ucy.ac.cy

[b] Dr. M. Fossépré, Dr. M. Leclercq, Dr. M. Surin
Laboratory for Chemistry of Novel Materials
University of Mons – UMONS
20 Place du Parc, B-7000 Mons (Belgium)
E-mail: mathieu.surin@umons.ac.be

Supporting information for this article is available on the WWW under <https://doi.org/10.1002/chem.202201497>

© 2022 The Authors. Chemistry - A European Journal published by Wiley-VCH GmbH. This is an open access article under the terms of the Creative Commons Attribution Non-Commercial License, which permits use, distribution and reproduction in any medium, provided the original work is properly cited and is not used for commercial purposes.

While in vitro G-quadruplexes readily assemble from ssDNA or RNA, in vivo, where they may exist in equilibrium with competing topologies (e.g., dsDNA, T-loop, etc), they are proposed to require the action of protein chaperons for folding.^[10] However, in light of their unusual thermodynamic and kinetic stability,^[11] their transient formation is believed possible under conditions of negative DNA supercoiling and molecular crowding caused by protein binding,^[12] such as those encountered in the course of replication, transcription and recombination events. Recent lines of evidence, stemming from the use of G-quadruplex-specific antibodies on cancer cells or tissues,^[13] or target-specific small-molecule-based bioimaging probes against G-quadruplexes in live cells,^[14] have suggested the in vivo occurrence of G-quadruplexes, thus intensifying the interest in developing appropriate drug candidates to exploit the untapped medicinal potential offered by these structures.

This interest is owed, predominantly, to the ways in which G-quadruplexes may potentially serve in anti-cancer capacities.^[15] Notably, the application of small-molecule ligands that drive the folding or induce stabilization of G-quadruplexes in the G-rich promoter regions of known oncogenes,^[16] ribosomal DNA regions,^[17] tandem telomeric sequences,^[18] or 5'-UTRs of mRNAs,^[19] has been correlated with arrest of transcription, ribosome biogenesis, telomerase-mediated telomere elongation and translation, respectively, with ensuing consequences for cancer cells. A handful of anti-cancer drug candidates resulting from such applications have now progressed to clinical trials.^[17] Based on these facts, G-quadruplexes define a novel target family for pharmaceutical intervention.^[20]

Of equal importance is the development of more sophisticated G-quadruplex-targeted chemical probes for efficient detection and monitoring of these labile entities in live cells,^[21] in order to shed light into their yet undisclosed cellular roles. In this direction, several research teams have been attempting to identify suitable binding motifs for targeting G-quadruplexes, whose interaction is accompanied by a detectable change in optical properties.

Apart from the numerous all-organic ligand families developed against G-quadruplexes,^[22] certain metal-based compounds exhibiting high stabilization ability towards G-quadruplexes have been described.^[23] Efficient metal-based G-quadruplex ligands typically exhibit: (i) extended aromatic chelators, some intrinsically planar (e.g., porphyrins), while others exploiting the organizational role of transition-metal cations with predisposition toward square planar (d^8 systems) or similar geometry; (ii) central cation involvement in cation-dipole interactions with G-tetrad carbonyls, in lieu of the physiological monovalent cation; and (iii) satisfactory aqueous solubility owing to the presence of at least one cationic (metal) center.

Platinum(II) has been prevalent in metal-based G-quadruplex ligands, owing to its d^8 electronic configuration favouring planarity in tetracoordinated complexes, which allows for π - π stacking with the terminal and solvent-exposed G-quartets. Additionally, the redox inertness of Pt(II) under physiological conditions combined with medium toxicity, the anti-cancer precedent provided by established Pt(II) drugs (e.g., cis-platin)

and, in certain cases, the desirable optical properties of Pt(II)-complexes, render Pt(II) particularly attractive. Successful examples of Pt(II)-based G-quadruplex binders comprise bi- or tridentate ligands such as phenanthroline,^[24] terpyridine,^[25] 2-(pyridin-2-yl)-1,10-phenanthroline,^[25d] 2,6-di(quinolin-2-yl)pyridine,^[25c,26] 2,4-di(pyridine-2-yl)pyrimidine,^[27] 2,6-bis(1H-benzo[d]imidazole-2-yl)pyridine,^[26,28] 2,6-di(1H-pyrazol-3-yl)pyridine,^[28] phenanthroimidazole,^[29] dipyrrophenazine,^[30] 7H-dibenzo[de,g]quinolin-7-one^[31] and salphen.^[32]

While numerous Pt(II)-complexes have been reported for G-quadruplex interaction, the uncertainty surrounding their cellular uptake, metal complex integrity and whether that is retained upon cellular entrance, as well as the issue of free metal cation-induced toxicity, remain major limitations to their applicability. To address these challenges, organometallic counterparts have been proposed. Examples in this category are still scarce, involving ligands such as 2-phenylpyridine,^[30] 2-phenyl-1,10-phenanthroline^[33] and 7H-dibenzo[de,h]quinolin-7-one.^[34] Such organometallic species enhance chemical stability thanks to their strong C–Pt bond, while some are neutral, thus favouring membrane permeability and reducing the possibility for electrostatic, non-specific association to negatively-charged cellular components.

The current study investigates a newly-synthesized class of 6-phenyl-2,2'-bipyridine derivatives as Pt(II) ligands, with the purpose of producing enhanced organometallic square planar G-quadruplex-interacting compounds, that benefit from the appendage of privileged peptide-mimetic side-chains. The 6-phenyl-2,2'-bipyridine $N^A N^C$ ligand has received much attention, in terms of the light-emitting properties of some of its simpler organometallic derivatives,^[35] which has led to its application in dye-sensitizing solar cells.^[36] Surprisingly, this ligand has not been systematically investigated in the context of G-quadruplex binder or optical probe design. The success of the structurally-related terpyridine-based Pt(II)-complexes as binders and modulators of various G-quadruplexes^[25] has prompted us to explore the more robust (2-([2,2'-bipyridin]-6-yl)phenyl)platinum(II) scaffold as a viable motif for G-quadruplex interaction. Our selection of side-chains/appendages was intended to influence its interaction mode with conformationally-distinct DNA secondary structures, such as the c-myc oncogene promoter parallel G-quadruplex and the telomeric hybrid and antiparallel G-quadruplexes, considered potential targets from an anticancer research standpoint, with other more common structures (dsDNA, ssDNA) serving as controls. Specifically, the use of peptide-mimetic (including chiral) components in the appendages, appears to enhance compound binding affinity and selectivity for c-myc, and to a lesser extent for telomeric DNA, despite the fact that these compounds comprise a neutral scaffold. Importantly, these Pt(II)-complexes exhibit remarkable and selective emission enhancements upon c-myc interaction, combined with significant c-myc stabilization capability, comparable or even superior to structurally-related, charged Pt(II)-complexes. Moreover, UV Resonance Raman (UVR) spectroscopy is applied herein as a powerful tool to probe the nature of the interactions, while a computational molecular docking simulation is employed to reveal the strong

influence of the Pt(II)-complex appendages on the binding modes, and how they dictate a preference toward alternative c-myc conformations.

Results and Discussion

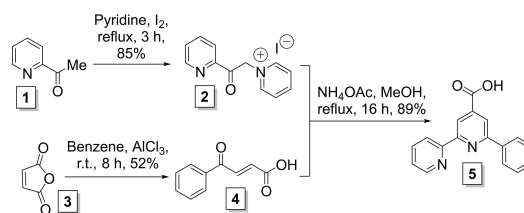
Selection of DNA targets

Three well-studied and topologically diverse G-quadruplexes were included in this study: The prototype parallel G-quadruplex of the c-myc oncogene promoter (myc2345-pu22, 5'-TGAGGGTGGGTAGGGTGGGTAA-3'), and the hybrid and basket-type antiparallel telomeric (22AG, 5'-AGGGTTAGGGTTAGGGTTAGGG-3') G-quadruplexes, favoured in K⁺- and Na⁺-rich conditions, respectively. c-Myc is found amplified in many cancer cell lines,^[37] while its protein product, a key transcription factor in oncogenesis, is considered 'undruggable'.^[38] The telomeric sequence is involved in genome stability while in cancer cells it serves as recognition site for telomerase, an enzyme responsible for cancer cell 'immortalization', by means of telomere elongation.^[39] These facts justify the need for developing new recognition motifs against these targets, to be applied both as DNA-level intervention agents and optical probes. Our study also employed self-hybridizing duplex ds26 (5'-CAATCGGATCGAATTCGATCCGATTG-3') and ssDNA polyT (5'-T₂₀-3'), as comparative controls.

Design and synthesis of organoplatinum compounds

The 6-phenyl-2,2'-bipyridine-based organoplatinum scaffold makes it possible to test whether neutral square planar organometallic species can be efficient for interaction, when supplemented with 'smart' appendages. Via chemical modification to peripherally introduce these diverse side-chains, it may be rendered capable of a combined interaction on terminal G-quartets, as well as loop- or groove-exposed moieties of G-quadruplexes. The current study aimed at generating 5 novel Pt(II)-compounds from this scaffold, which incorporate peptide-like features in their side-chains, in an attempt to mimic interactions and/or steric effects of known G-quadruplex-binding proteins or peptides.^[40] The 4-position of the central pyridine of the scaffold was chosen for chemical modification with either bulky hydrophobic, polar cyclic amine-based, heteroaryl or chiral cyclic moieties, that represent a wide range of possible interacting elements in G-quadruplex-recognizing peptides, thus enhancing possibility for favourable modes of binding.

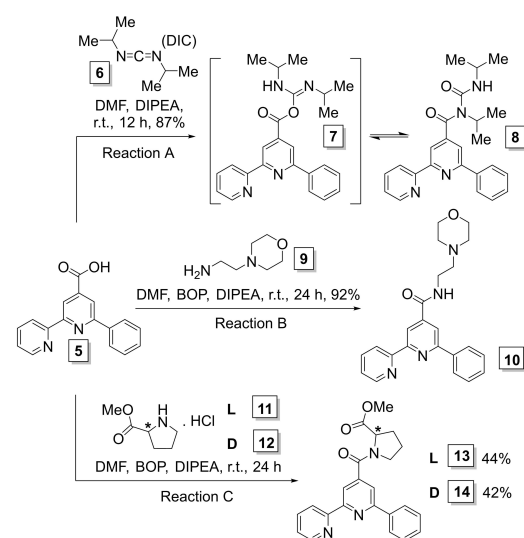
All derivatives of the 6-phenyl-2,2'-bipyridine N^NC ligand included in this study were envisaged to derive from a common precursor, 6-phenyl-[2,2'-bipyridine]-4-carboxylic acid (5), which was constructed from simple, commercially available building blocks (Scheme 1). First, 2-acetylpyridine (1) was converted to 1-(2-oxo-2-(pyridin-2-yl)ethyl)pyridin-1-ium iodide (2, 85% yield), upon treatment with iodine in pyridine, at reflux.^[41] In parallel, maleic anhydride (3), under Friedel-Crafts conditions



Scheme 1. Synthesis of 6-phenyl-[2,2'-bipyridine]-4-carboxylic acid (5).

(AlCl₃ in benzene), afforded 4-oxo-4-phenylbut-2-enoic acid,^[42] with the (*E*)-geometric isomer (4) being isolated after recrystallization, in 52% yield. An equimolar mixture of 2 and 4 was submitted to reflux in the presence of NH₄OAc in MeOH, leading, via cyclocondensation/aromatization, to formation of 6-phenyl-[2,2'-bipyridine]-4-carboxylic acid (5), in 89% yield.^[43]

While compound 5 has been previously validated as tridentate ligand for metal cations,^[35a] the aim of the current study was to further derivatize this precursor on the carboxy-position, in order to gain access to novel ligands, in terms of their peripheral side-chains and resulting G-quadruplex target-interacting capabilities. A facile way for derivatization was amide formation. In the course of screening a number of carbodiimide- and phosphonium-based activating reagents for amide coupling, in combination with various solvents and bases, we serendipitously identified the generation of a persistent, silica chromatography-stable adduct, in the reaction between 5 and diisopropylcarbodiimide (DIC, 6) in DMF, in the presence of diisopropylethylamine (DIPEA) (Scheme 2, reaction A). This product formed regardless of the presence or absence of primary amine nucleophile. NMR analysis was consistent with the structure of carbamoyl amide 8, which was later unambiguously confirmed by the crystal structure of its respective organoplatinum complex (see next section). The formation of 8 can be explained via an intermolecular *N,O*-rearrangement of



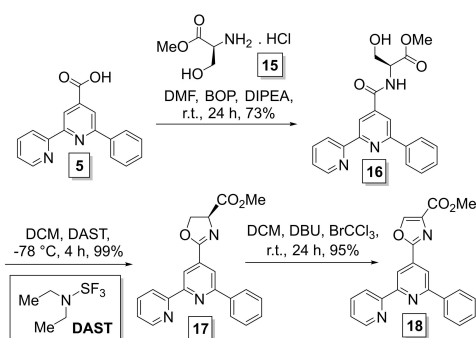
Scheme 2. Syntheses of novel amide-type ligands (8, 10, 13 and 14), employed in this study.

intermediate **7**. Compound **8**, isolated in 87% yield, was deemed interesting for further use as a ligand, since it provides sterically-hindered, rotationally-constrained hydrophobic segments that resemble side chains of aliphatic amino acids found in several G-quadruplex-interacting peptides.^[40]

By selecting benzotriazol-1-yloxytris(dimethylamino) phosphonium hexafluorophosphate (BOP) as the optimal activating reagent for amide coupling, in DMF, in presence of DIPEA, we proceeded to synthesize 3 additional amide-type ligands. Ligand **10** was the amide product obtained in excellent yield (92%), when primary amine **9** was employed, introducing a morpholino-tail on the end of a 2-carbon chain (Scheme 2, reaction B). Amines of similar type, capable of protonation under physiological conditions, have been previously validated as appendages on extended aromatic scaffolds for G-quadruplex targeting,^[14b,25b,d,33] aiming to enhance overall binding affinity by contributing electrostatic interactions with nucleic acid sugar-phosphate backbones. This approach mimics the behaviour of basic residues in G-quadruplex-targeting peptides.^[40]

Additionally, via reaction of **5** with (in house-prepared^[44]) L- and D-proline methyl ester hydrochloride salts (**11** and **12**, respectively), the enantiomeric proline imide ligands were obtained (Scheme 2, reaction C) in modest yields (**13** in 44% and **14** in 42%, respectively). These offer the possibility of studying the effect of ligand chirality on the interaction with G-quadruplexes, constituting a novelty in metal-based binder design, as very few enantiomeric examples have been reported in the literature against G-quadruplexes to date, typically bimetallic that exhibit axial chirality.^[45] In the proline imide case, the chiral center is positioned adjacent to the junction of the appendage with the plane of the scaffold, rendering it capable of playing a role in the expected interaction with a terminal G-quartet and other moieties in its proximity.

Finally, in order to develop a ligand with extended conjugated π -system, we applied a 3-step route from carboxylic acid **5**, leading to oxazole-containing compound **18** (Scheme 3). Amide coupling of **5** with serine methyl ester hydrochloride^[44] (**15**) afforded intermediate **16** (73% yield). This underwent dehydration/cyclization, enabled by DAST in DCM at -78°C ^[46] to yield oxazoline **17** (99% yield), which was, in turn, aromatized to the desired oxazole (**18**, 95% yield) upon

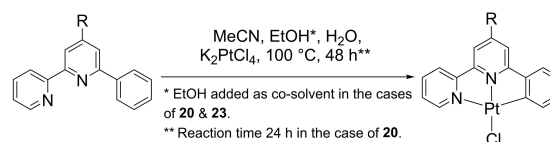


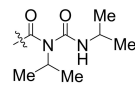
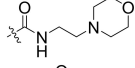
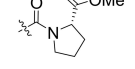
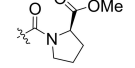
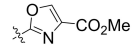
Scheme 3. Synthetic route employed in this study for generation of an oxazole-containing ligand (**18**).

treatment with BrCCl_3 in DCM, in the presence of DBU.^[47] Pyridyl-oxazoles and other N,O-based 5- and 6-membered heteroaryl systems have been highlighted in relevant work by several teams including ours,^[48] as privileged components for the construction of G-quadruplex-targeting molecules, due to their small ring size, hydrophobicity and hydrogen-bonding potential.

All new ligands generated from **5** (compounds **8**, **10**, **13**, **14** and **18**) were subsequently submitted to platination by refluxing with K_2PtCl_4 in $\text{CH}_3\text{CN}-\text{H}_2\text{O}$ for 24 or 48 h (Scheme 4).^[49] This mixed solvent (occasionally supplemented with EtOH) was necessary to solubilize all reactants at the start of the reaction.

Elimination of HCl afforded a series of square planar organoplatinum compounds (**19–23**, respectively), in which the 4 coordination sites on the Pt(II) center are occupied by the tridentate ($\text{N}^3\text{N}^1\text{C}$) ligand and a chloride anion. Products **19–22** were obtained upon solvent evaporation, extraction in a chloroform–water system and recovery from the organic phase. Product **23** precipitated during the reaction and was collected by filtration. All products were further purified by recrystallization or wash-centrifugation, and obtained in the form of (red, orange or yellow) small crystals or fine powders, in high yields (86–91%). The success of each complexation was confirmed by the disappearance of one aromatic signal in the ^1H NMR spectrum relative to the free ligand, as well as a significant shift of all remaining aromatic signals and loss of symmetry of the Ph ring. MS-MALDI-TOF confirmed the expected masses and UV-vis spectra showed a new weak peak around 450 nm, corresponding to a d-d transition of the complex. The structure of compound **19**, was also confirmed by X-ray crystallography (see next section).



Free ligand	Pt(II)-complex	Side-group R	Yield %
8	19		91
10	20		87
13	21		89
14	22		91
18	23		86

Scheme 4. Platination reaction generating scaffold-neutral, square-planar organoplatinum complexes.

Single-crystal XRD of compound **19**

Suitable single crystals of organoplatinum compound **19** were formed after slow evaporation of a solution in CH₃CN and a crystal structure was obtained by X-ray diffraction. This compound crystallizes in the orthorhombic space group *Pbca* with 8 molecules in each unit cell (Supporting Information, Table S1). The asymmetric unit of **19** consists of one neutral molecule, where the Pt(II) center adopts a distorted square planar coordination geometry. The coordination sphere of the Pt(II) center consists of a DIC-derived tridentate N⁴N⁴C ligand and a terminally ligated Cl[−] anion. The maximum deviation of Pt1 from the coordination plane (N1–N2–C16–Cl1, Figure 1A) is 1.06°. The tridentate ligand bite angle was found to be 161.7° (Supporting Information, Table S5), in agreement with related terpyridine Pt(II)-complexes reported in the literature.^[25d] The aromatic core of **19** is nearly planar, with most non-hydrogen atoms lying on the same plane, however, a slight distortion is observed for the carbon atoms of the central pyridine ring, which deviate from planarity [deviation from plane C7 (0.18 Å), C8 (0.23 Å), C9 (0.13 Å)]. Two molecules of **19** are related through an inversion center and interact through π - π stacking between the phenyl ring of one and the central pyridine ring of the other (Figure 1B). These interactions are relatively strong considering that the distance between the aromatic rings ranges from 3.244 Å to 3.380 Å, and are comparable to terpyridine- and 2-phenyl-1,10-phenanthroline-based Pt(II)-complexes.^[25b,d,33] Moreover, the dimers of **19** interact through N–H...Cl hydrogen bonds (N4–Cl1 distance 3.391 Å) between the terminally ligated Cl[−] anion and the nitrogen atom (N4) of the *N*-acyl-urea group (Figure 1C), essentially forming 1-dimensional chains along the *b*-axis.^[50]

Binding affinities of Pt(II)-complexes for various DNAs, assessed via UV-vis and fluorescence titrations

Considering reversible interactions, the binding affinities of the synthesized Pt-compounds toward a series of DNAs exhibiting

diverse topologies were assessed, by means of two independent methods, UV-vis and fluorescence titrations. The binding studies included: *c*-myc/K⁺, an oncogene promoter of parallel G-quadruplex fold; 22AG/K⁺, a telomeric sequence of hybrid G-quadruplex fold; 22AG/Na⁺, folding as antiparallel basket-type G-quadruplex; ds26, a self-hybridizing duplex; and polyT, a single strand with no organized secondary structure (CD spectra in Supporting Information, Figures S44–47). A direct fit approach, employing a non-linear sigmoidal model to correlate the working peak maximum (UV-vis) or normalized maximum (fluorescence) with the variable DNA concentration was applied, in order to determine the association constants ($K_a = 1/K_d$), for which our model afforded good convergence ($R^2 \geq 0.99$). The obtained results are presented in Table 1 and graphically in Figure 2.

In the UV-vis titrations, a 30 μ M solution of each Pt-compound in 50 mM Tris.HCl buffer (pH 7.4), supplemented with 100 mM KCl or NaCl, was titrated by stepwise addition of aliquots of a pre-organized DNA solution (concentration in the range of 0.57–2.15 mM) in the same buffer. A strong interaction of **19**–**22** with *c*-myc manifested as hypochromism along with significant bathochromism (red shift of ~ 15 nm) of the working peak maximum (initially at 340 nm) (Supporting Information, Figures S3–6). Such behaviour is consistent with a π - π stacking mode of binding, as previously suggested for interaction of planar ligands with parallel G-quadruplexes.^[51] Moreover, the presence of isosbestic points in UV-vis titrations with *c*-myc was indicative of a single equilibrium. Hypochromism and bathochromism were less evident in UV-vis titrations of **19**–**22** with the two telomeric G-quadruplexes and ds26 (Supporting Information, Figures S7–18), hinting on a weaker interaction. Interactions of **19**–**22** with polyT were so negligible that did not allow convergence of the model for the UV-vis data. Compounds **19**–**22** demonstrated higher binding affinities for *c*-myc, compared to all other DNAs studied, with K_a values in the range of 2.3 – 5.2×10^5 M^{−1} (Table 1).

These are comparable to Pt(II)–terpyridine complexes that bear cyclic amine side-chains.^[25b] The binding selectivities (based on ratios of K_a values) of the members of this compound

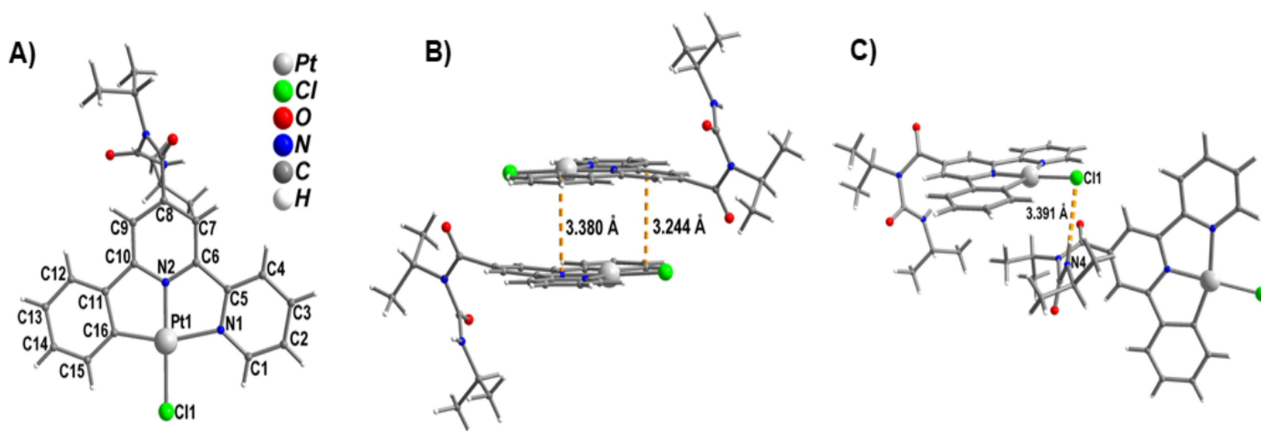
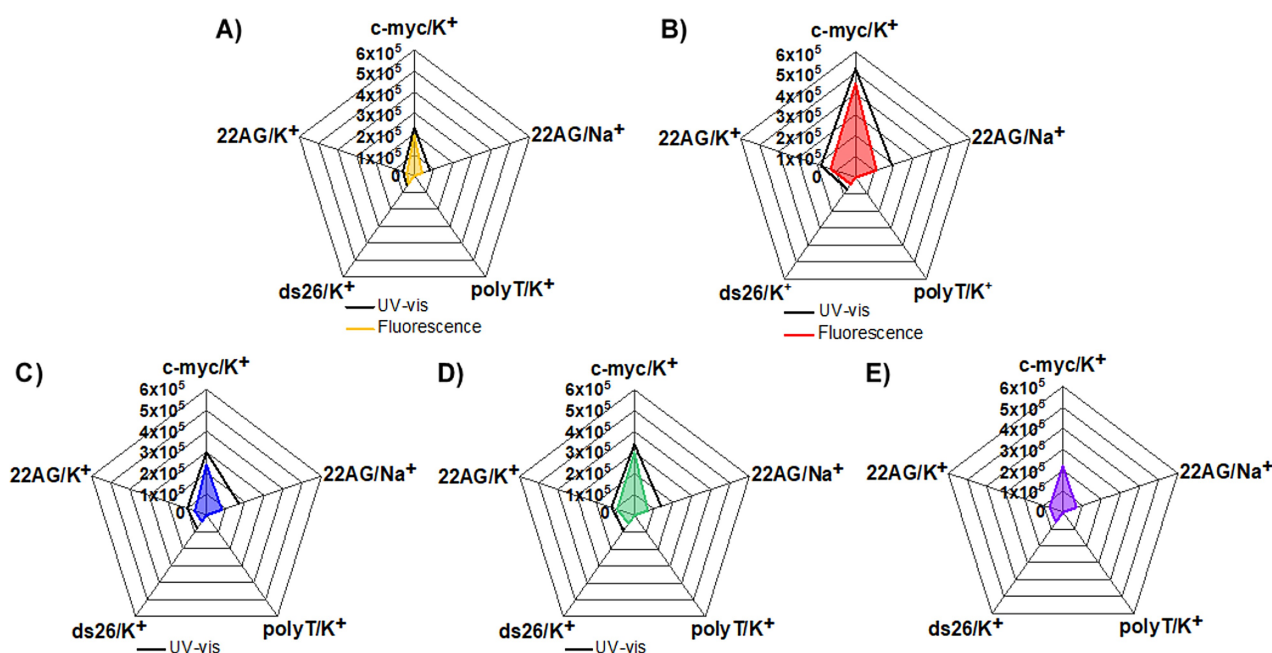


Figure 1. X-ray crystal structure of organoplatinum compound **19**. A) Single molecule. B) Antiparallel π - π interaction of two neighbouring molecules, side view, showing selected distances. C) Side-chain interaction with chloride of a second molecule, showing N–H...Cl bonding distance.

Table 1. Association constants (K_a) for interactions between Pt(II)-complexes and DNAs included in this study, as determined by: A) UV-vis titrations (in 50 mM Tris.HCl buffer, pH 7.4, containing 100 mM KCl or NaCl); and B) Fluorescence titrations (in 10 mM Li-cacodylate buffer, pH 7.2, containing 100 mM KCl or NaCl).

Entry	Pt(II)-Complex	c-myc/ K^+ (parallel G4)		22AG/ K^+ (hybrid G4)		22AG/ Na^+ (antiparallel G4)		ds26/ K^+ (duplex)		poly-T/ K^+ (single stranded)	
		K_a ($\times 10^5 M^{-1}$) [A]	K_a ($\times 10^5 M^{-1}$) [B]	K_a ($\times 10^5 M^{-1}$) [A]	K_a ($\times 10^5 M^{-1}$) [B]	K_a ($\times 10^5 M^{-1}$) [A]	K_a ($\times 10^5 M^{-1}$) [B]	K_a ($\times 10^5 M^{-1}$) [A]	K_a ($\times 10^5 M^{-1}$) [B]	K_a ($\times 10^2 M^{-1}$) [A]	K_a ($\times 10^2 M^{-1}$) [B]
1	19	2.3 ± 0.1	1.9 ± 0.1	0.6 ± 0.2	0.4 ± 0.1	0.8 ± 0.4	0.4 ± 0.1	0.6 ± 0.3	0.5 ± 0.2	ND ^[b]	0.4 ± 0.3
2	20	5.2 ± 0.3	4.5 ± 0.2	1.8 ± 0.5	1.3 ± 0.1	1.9 ± 0.7	1.1 ± 0.2	0.7 ± 0.3	0.4 ± 0.1	ND ^[b]	9.6 ± 7.6
3	21	3.0 ± 0.1	2.4 ± 0.2	1.0 ± 0.3	0.6 ± 0.1	1.7 ± 0.7	0.8 ± 0.1	0.8 ± 0.3	0.4 ± 0.1	ND ^[b]	3.0 ± 2.5
4	22	3.4 ± 0.1	3.0 ± 0.2	1.2 ± 0.3	0.9 ± 0.2	1.4 ± 0.5	0.7 ± 0.2	0.9 ± 0.3	0.5 ± 0.1	ND ^[b]	3.7 ± 3.0
5	23	ND ^[a]	2.2 ± 0.3	ND ^[a]	0.7 ± 0.3	ND ^[a]	0.7 ± 0.2	ND ^[a]	0.6 ± 0.1	ND ^[a,b]	3.5 ± 2.8

[a] Not determined due to precipitation of compound 23 in the course of the titration. [b] Not determined due to negligible interactions that did not allow model convergence.

**Figure 2.** Radar chart allowing comparison of association constants (K_a) as determined by UV-vis titrations (black open line) and fluorescence titrations (coloured closed line, filled). Each angle corresponds to one of the DNAs included in this study. Units are M^{-1} . A) 19; B) 20; C) 21; D) 22; E) 23.

class for c-myc were 2- to 4-fold higher compared to both the hybrid and antiparallel topologies of 22AG, and 4- to 7.5-fold higher compared to duplex ds26 (Figure 2).

Model convergence indicated that compounds 19–22 interact with c-myc in a 2:1 Pt-complex-to-DNA stoichiometry, consistent with an end-stacking mode at both solvent-exposed terminal G-quartets of this parallel G-quadruplex. This resembles the interaction mode reported for other types of planar binders of c-myc.^[33,52] Notably, stoichiometry becomes 1:1 for all other DNAs studied, which could reflect a steric hindrance imposed by the longer loop of 22AG or a difficulty encountered by these bulky ligands for intercalative binding in ds26.

Each distinct set of association constants (K_a) corresponding to one DNA, comprises values of the same order of magnitude, suggesting a major contribution to binding from the common planar organometallic scaffold of 19–22. Notably, the c-myc dataset exhibits the broadest distribution of K_a values, implying

that it is especially with c-myc that the diverse side-chains exert an important role, by interacting with domains of the G-quadruplex other than terminal G-quartets, such as loop and groove residues. Affinity-wise, compound 20, bearing the ionizable morpholine appendage, was the most potent binder against c-myc ($K_a = 5.2 \times 10^5 M^{-1}$), presumably due to the contribution of a protonated side-chain in terms of electrostatic and/or H-bonding interactions. Predictably, the most sterically hindered compound (19) had the weakest binding ($K_a = 2.3 \times 10^5 M^{-1}$). Interestingly, the two enantiomeric proline-based Pt-compounds (21 and 22) exhibited a subtle but statistically significant deviation from each other, with the D-isomer (22) appearing somewhat more potent against c-myc. This difference can be correlated with the proximity of the stereogenic center to the compounds' planar scaffold, in conjunction to steric constraints imposed by the proline ring, which together may dictate alternative orientations for the 2 enantiomers in

their contacts with residues surrounding the external G-tetrads (see molecular simulations section).

The results for 22AG/K⁺, 22AG/Na⁺ and ds26 showed that the compounds were not as distinctly-behaved in their interactions with each of these DNAs, suggesting that the role of the side-chains, as well as their contribution to binding affinity, may be more limited in these cases (see Raman study with other DNAs, Supporting Information).

Pt-compound **23** exhibited abnormal behaviour in UV-vis titrations, with formation of solid precipitates that prevented experiment completion. This may be rationalized in terms of the extended π -system and high hydrophobicity of **23**, which renders the compound capable of significant π - π stacking. The propensity of **23** for π - π stacking also became evident from the chemical shifts of aromatic proton signals, observed in variable temperature and variable concentration NMR experiments (vt- and vc-NMR, see Supporting Information, Figures S1–2).^[53] It is reasonable to hypothesize that the studied DNAs serve as a template to drive the self-aggregation of compound **23** molecules.

Fluorescence titrations were deemed necessary, as a complementary method to allow study of the interactions at lower concentrations of both Pt-complexes and DNA, in order to corroborate the findings of UV-vis titrations, assess the affinity of compound **23** for the DNAs, as well as enable collection of data with the polyT DNA control.

In fluorescence titrations (Supporting Information, Figures S19–43), a series of mixtures corresponding to various molar ratios of Pt-compound and DNA was prepared, to the same total volume and a final Pt-compound concentration fixed at 5 μ M. These mixtures corresponded to ‘snapshots’ of an actual titration. Solutions were buffered with 10 mM lithium cacodylate (pH 7.2), supplemented with 100 mM KCl or NaCl. Excitation took place at 320 nm, while emission of the Pt-complexes occurred in the range of ~575–595 nm, depending on the side-chain type. While the free Pt-complexes have very low emission in aqueous buffers, the fluorescence intensity of the mixtures systematically increased with the increase of DNA-to-Pt-complex ratio, likely due to the exposure of the complexes to the solvent-protected environment provided by DNA binding surfaces.

K_a values determined via fluorescence titrations, albeit somewhat suppressed, were found (within experimental error) to be comparable to UV-vis results and generally followed the same trends (Table 1 and Figure 2). Compounds **19–22** ranked in the same order in their interaction with c-myc. Their binding selectivities for c-myc vs. the other DNAs were determined to be higher by fluorescence (3- to 5-fold higher vs. the two forms of 22AG; 4- to 10-fold higher vs. ds26).

The aggregation of **23** was avoided in fluorescence titrations, and its binding affinities to the various DNAs were determined. The oxazole-based **23** appeared comparable to the weakest binder (**19**) against c-myc (with $K_a = 2.2 \times 10^5 \text{ M}^{-1}$), which was, nonetheless, its preferred binding partner out of the DNA structures tested. Compound **23** showed similar affinities with the proline-based compounds (**21** and **22**) in its interaction with the two topologies of 22AG and with ds26. However, its

selectivity for c-myc vs. 22AG (both forms) and ds26 was rather modest (3-fold and 4-fold, respectively) when compared to counterparts **19–22**.

Finally, all five Pt-complexes showed negligible affinity for polyT DNA (in the order of 10^1 – 10^2 M^{-1} , 3–4 orders of magnitude lower than for G-quadruplexes), demonstrating a clear selectivity for organized, in particular G-quadruplex, DNA structures.

Emission enhancement of Pt(II)-complexes upon DNA interaction

The emission spectra of the five Pt-complexes were recorded in the absence and presence of excess DNA (5 equiv.), in 10 mM Li-cacodylate buffer, pH 7.2, containing 100 mM KCl or NaCl (first and last curve in fluorescence titrations, Supporting Information, Figures S19–43). As a result of their interaction with DNA, this series of Pt-compounds exhibit ‘light-up’ behaviour, which may be of interest for the development of G-quadruplex-targeted optical probes. Emission enhancement for compounds **19–22** was more pronounced in the presence of c-myc G-quadruplex, while the same compounds were significantly less responsive to the hybrid and antiparallel G-quadruplex topologies of 22AG, to the duplex ds26 and to polyT DNA (Figure 3). Compound **23** was less discriminatory against the various DNAs. The emission enhancements of **19–22** observed with c-myc were notably higher compared to other organoplatinum complexes, for which ‘light up’ effects have been reported.^[33] The remarkable optical selectivity of **19–22** for c-myc, in conjunction with their unusual hydrophobicity, could provide a basis for development of a new class of cell-permeable optical probes for c-myc detection.

The optical response of the compounds to c-myc was strongly dependent on the nature of their side-chain. The ranking of the compounds from strongest to weakest emission enhancement with c-myc was: **21** > **20** = **22** > **19** > **23** (Figure 3). The differential behaviour of the Pt-complexes with regard to their optical properties, highlights the importance of the side-

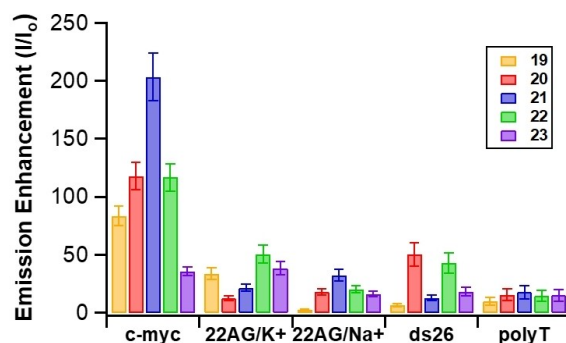


Figure 3. Emission enhancement (I/I_0) of Pt-complexes at 1:5 molar ratio of Pt-complex-to-DNA, in 10 mM Li-cacodylate buffer (pH 7.2), containing 100 mM KCl or NaCl. [Pt-complex] = 5 μ M. Optical selectivity for c-myc is exhibited by compounds **19–22**.

chains in dictating ligand orientation and solvent exposure during the interaction with c-myc.

Smaller differences between the Pt-complexes' optical responses were observed with 22AG and ds26 as well, with a different complex being predominant in each case (i.e., **22** with 22AG/K⁺; **21** with 22AG/Na⁺; **20** with ds26) (Figure 3).

Stabilization induced to c-myc by Pt(II)-complex binding, determined via circular dichroism (CD) DNA-melting study

Given the promising performance of some of the synthesized Pt-compounds on c-myc, both in terms of binding affinity and selectivity, as well as optical response and selectivity, we focused all additional studies on this particular G-quadruplex structure.

We next set out to determine any stabilizing effects of the Pt-complexes on c-myc. The melting temperature, T_m , provides a measure of the thermodynamic stability of a G-quadruplex, while the difference of T_m values (ΔT_m) in the presence and absence of an interacting ligand, is indicative of the stabilizing effect of that ligand. A protocol involving CD spectroscopy-monitored DNA thermal denaturation (melting)^[54] was employed for assessing T_m values of both the free and ligand-bound c-myc, taking into account that c-myc maintains a parallel topology throughout the experiment. CD was selected over a FRET alternative,^[55] in order to exclude any possibility of Pt-complex interference with the absorption and/or emission of the dyes routinely used in FRET G-quadruplex melting studies. A 5 μ M c-myc solution in 10 mM Li-cacodylate buffer, pH 7.2, containing 99 mM LiCl and 1 mM KCl, was employed, in order to evaluate ligand-induced stabilization on a loosely pre-organized c-myc G-quadruplex, that allows ample window to observe the change. The DNA solution was submitted to a temperature gradient, from 20 to 95 °C, at a rate of 1 °C min⁻¹, with the CD spectrum being recorded at 5 °C intervals. Molar ellipticity (θ), corresponding to the maximum of the positive peak appearing at $\lambda=265$ nm in the CD spectrum of c-myc, which is characteristic of a parallel G-quadruplex (see Supporting Information, Figure S44), was recorded. It was normalized by dividing with the initial molar ellipticity value at the starting temperature of the experiment, thus setting initial normalized θ equal to 1. The normalized θ values were plotted against temperature (for DNA melting curves, see Supporting Information, Figure S52). Fitting of a non-linear, sigmoidal model to the data allowed determination of T_m for (free or ligand-bound) c-myc (at normalized $\theta=0.5$).

In all cases, the addition of Pt-complex led to a significant increase of T_m compared to free c-myc ($T_{m,c-myc}=63.8$ °C), indicating helix stabilization. The determined ΔT_m values are shown in Figure 4. They are superior to those of Pt-terpyridine counterparts on c-myc,^[25e] thus downplaying the need for a charged scaffold in order to achieve significant thermodynamic stabilization of G-quadruplexes. However, the appendage of a peripheral (positively) ionizable amino-side chain to the planar scaffold indeed proved to be an important component of ligand design, with morpholino–Pt-complex **20** exhibiting an impres-

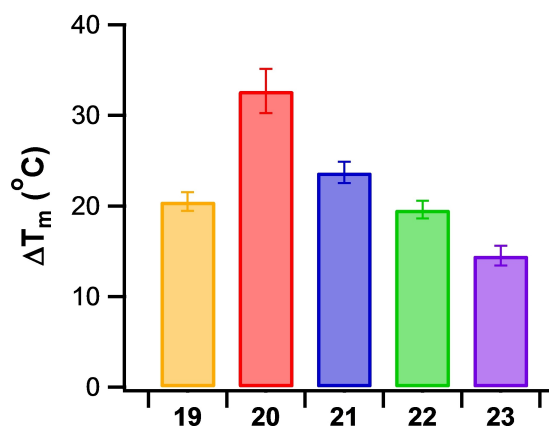


Figure 4. Pt-complex-induced stabilization of c-myc G-quadruplex (ΔT_m), determined via circular dichroism (CD)-based DNA melting study. Mixtures of c-myc and Pt-complex in 5 μ M and 25 μ M concentrations, respectively, were employed, buffered with 10 mM Li-cacodylate, pH 7.2, containing 99 mM LiCl and 1 mM KCl.

sive $\Delta T_m > 30$ °C. It is presumed that additional interactions gained due to the presence of the amine make an important contribution toward G-quadruplex stabilization. This finding is aligned with the superior binding affinity of this ligand for c-myc, determined via UV-vis and fluorescence titrations, as well as the results of the docking study that follows. The enantiomeric ligands **21** and **22** exhibited a modest difference in ΔT_m , with the L-enantiomer (**21**) appearing somewhat superior over the D-enantiomer (**22**), in enhancing c-myc stability (23.7 vs. 19.6 °C). This suggests that the higher binding affinity of **22** for c-myc G-quadruplex does not necessarily translate into a stronger stabilizing effect, as compared to **21**. The DIC-derived Pt-complex (**19**) exhibited a stabilizing ability intermediate of the two proline-Pt-complexes (20.5 °C), suggesting that despite its significant steric hindrance, favourable interactions within the loops or grooves may still be developed. Finally, the oxazolino–Pt-complex **23** appeared to have the lowest stabilizing ability of this set, with a ΔT_m around 14 °C, well correlating with its lower affinity for c-myc.

In the cases of Pt-ligands **19–22**, a second inflection point may be observed at the initial section of the melting curves, around 30–50 °C (Supporting Information, Figure S52), which is not present in the DNA-only case. This may be attributed to an interaction of the various side-chains, with sites of the G-quadruplex other than the G-quartet-based core (e.g., loop or groove-exposed residues), which also participate in the overall stabilization of the helical structure. These interactions are expected to be weaker than the forces maintaining the stability of the G-tetrad core, hence they break up at lower temperatures.

UV resonance Raman (UVR) investigation of interactions between Pt(II)-complexes and DNAs

UV resonance Raman (UVR) experiments were performed with excitation at 266 nm, a wavelength between the absorption maximum of the c-myc G-quadruplex (at 256 nm) and a maximum of the Pt-complexes (at 273 nm). This wavelength was selected for signal enhancement mostly owed to the DNA bases, since c-myc DNA exhibits extinction coefficient $\epsilon = 228700 \text{ L}\cdot\text{mol}^{-1}\cdot\text{cm}^{-1}$, approximately one order of magnitude

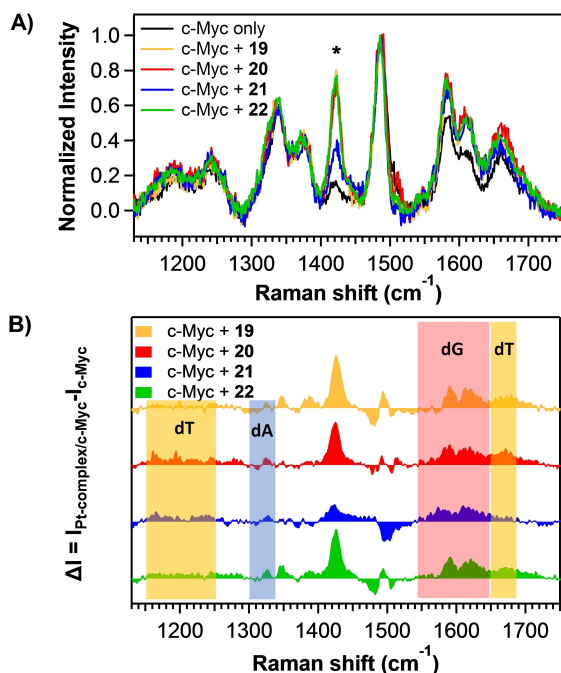


Figure 5. A) UVR spectra of c-myc G-quadruplex alone and in mixture with Pt-complexes, with excitation at 266 nm. The asterisk denotes a solvent band (DMSO). B) Difference Raman spectra of Pt-complexes with c-myc, after subtraction of the Raman spectrum of c-myc at 266 nm (19: yellow; 20: red; 21: blue; and 22: green). The band at 1420 cm^{-1} corresponds to the solvent (DMSO). The highlighted spectral regions correspond to the bands used in quantifying the changes upon interaction between the Pt-complexes and c-myc in Figure 6.

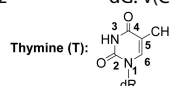
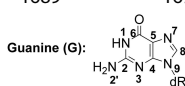
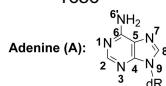
higher than that of the Pt-compounds (see Supporting Information, Figures S53–54). Only the four Pt-complexes (19–22), which were deemed more promising based on c-myc affinity, binding selectivity and optical response considerations, were included in the UVR study.

Excitation at 266 nm probes the structure of DNA and thus helps confirm the existence of the G-quadruplex helix in c-myc, as well as observe structural changes upon addition of the Pt-complexes. The UVR spectra observed for c-myc (Figure 5A) agree with literature,^[56] and contain contributions from guanines, adenines and thymines (see Table 2 for band assignments). Bands observed at ~ 1485 , 1580 and 1608 cm^{-1} correspond to vibrations in the guanine ring involving nitrogen atoms (C8N9 and N7C8 stretching, N2'H bending, and N1H bending, respectively). Therefore, these bands are sensitive to shifts upon Hoogsteen base pairing and consequently to any disruptions or enhancement of the interbase bonding. Two other bands that can provide information about the conformation of guanine-rich sequences are those at 1319 and 1337 cm^{-1} . The ratio of the intensity of these two peaks works as an indicator of the percentage of guanosine nucleosides that are in *anti* and *syn* orientation (C2'-endo/*anti* and C2'-endo/*syn*), which can help elucidate the percentage of parallel and antiparallel G-quadruplex helix in the DNA.^[56–58] However, the presence of adenines in the loops of c-myc with strong bands in the same region overshadows the contribution of these bands. Thymine, also present in the loops, contributes two bands in this spectral region at 1372 and 1660 cm^{-1} (C5–CH₃ deformation and C4=O stretching, respectively).^[56,59] Overall, the position of the aforementioned key bands observed in the UVR spectrum of c-myc (Figure 5A and Table 2) indicates that c-myc adopts a G-quadruplex conformation, which is preserved in the presence of Pt(II)-complexes.

However, distinct differences are observed in the UVR spectra upon addition of the Pt-complexes to the c-myc solution, that can be instructive for the interactions that develop between them. Normalization of the UVR spectra with respect to the intensity of the guanine band at $\sim 1485 \text{ cm}^{-1}$ (Figure 5A) and subtracting the spectra before and after adding the Pt-complexes illustrates changes in intensity and band

Table 2. Raman bands observed in the 266 nm UVR spectra of c-myc and its mixtures with Pt(II)-complexes. Inset: Nucleobase numbering.

Entry	Raman shift [cm^{-1}]					Vibrational mode description
	c-myc	+19	+20	+21	+22	
1	1244	1241	1243	1241	1241	dT: N3H def, v(CN)
2	1319	1318	1319	1319	1319	dA: v(C8N9, C2N3) purine ring
3	1338	1338	1338	1339	1339	dA: v(C5N7, N7C8) imidazole ring
4	1372	1373	1373	1371	1373	dT: C5–CH ₃ def
5	1421					dA: v(N1C6)
6	1486	1486	1487	1486	1486	dG: v(N7C8) Hoogsteen H-bond, v(C8N9), δ C8H
7	1512	1511	1512	1511	1510	dA
8	1581	1582	1582	1582	1581	dG: δ N2'H, H-bond
9	1608	1610	1612	1613	1612	dG: δ N1H, H-bond, v(C2N)
10	1661	1660	1661	1659	1660	dT: v(C4=O), H-bond, v(C5=C6)
11	1688	1692	1686	1689	1692	dG: v(C6=O), H-bond



position more clearly, providing direct information on the moieties of each base that are involved (Figure 5B). It is important to note that salts such as sodium sulfate, often used (in relatively large concentrations) as internal standards to monitor intensity changes in the RR bands, were avoided here in order to ensure that no conformational changes to the G-quadruplex structure are due to the ionic strength of the solution. This necessitates use of one of the DNA bands for normalization (the 1485 cm⁻¹ band here) which, however, assumes that this particular band does not undergo any intensity changes upon interaction with the Pt-complexes. The Pt-complexes do not contribute to the UVR spectra in this spectral region, therefore, any changes observed in the spectra of the small molecule/DNA complexes are solely attributed to the DNA bases.

In all cases, we observe intensity increases for the bands at 1582, 1608 and 1661 cm⁻¹ that correspond to guanine and thymine modes. Band intensity variations are indicators of perturbation in the environment of the various bases due to the interaction between the binder and the helix. The increased intensity of the 1582 and 1608 cm⁻¹ bands that correspond to guanine modes reveals an interaction between the Pt-complexes and the guanine tetrads, which could occur either at the end of the helix (end-stacking), or between guanine tetrads through classical intercalation.^[60] However, the observed hypochromism of the UV-vis absorption spectra of the Pt-complexes upon DNA addition (see Supporting Information, Figures S3–6) point to end-stacking interactions. Hypochromism in the absorption due to base stacking is expected to lead to reduction in RR band intensity. However, as in our case an independent internal standard was not used, the increase in intensity cannot be associated to intercalation between the tetrads. Similar intensity changes were observed in the work of Di Fonzo et al. upon end-stacking of BRACO-19 to c-myc.^[56]

Intensity changes that varied depending on the Pt-complex used were also observed for the thymine carbonyl band at 1661 cm⁻¹. This could be related to a change in the vibrational coupling between the base and sugar vibrations^[61] due to a stacking interaction of thymine in the loops of the G-quadruplex with the Pt-complex core, that results in the modification of the dihedral angle between the base and sugar. Some evidence exists in the docking simulations described below that this dihedral angle varies in the most stable conformers, depending on the side chain of the Pt-complex, from *syn* for compounds **20** and **22** to *anti* for **19** and **21**.

The intensity increase of the guanine bands is accompanied in all cases by a prominent shift in the 1608 band to 1613 cm⁻¹. This N1H bending vibration is sensitive to Hoogsteen hydrogen bonding, and displacement to higher wavenumbers indicates the stabilization of the quadruplex helix through 'end-stacking' interaction. However, this shift appears higher than what is usually observed for G-quadruplexes, so it is possible that another interaction is at work in this spectral region. Adenine, present in c-myc, also possesses a band at 1604 cm⁻¹ assigned to the NH₂ scissoring. Even though the intensity of this mode is expected to be lower than the N1H bend of guanine, it is possible that the shift we observe here is due to hydrogen

bonding of the exocyclic NH₂ group to the side chain of the Pt-complex (see docking simulations below) leading to an upshift of this band. In addition, the difference spectra of complexes **19**, **20** and **22** show a slight downshift of the dG N7C8 stretching band at 1485 (~1 cm⁻¹ as seen from the UVR spectra) leading to a -/+ peak pair (Figure 5B). This band is also sensitive to Hoogsteen hydrogen bonds, with the downshift further indicating that the hydrogen bonds are perturbed due to the stacking interaction of the Pt-complex molecules with c-myc.

Although the spectrum of complex **21** (L-enantiomer) shows an overall similar behavior as the other complexes regarding interactions with the guanine base pairs, the interactions with adenine and thymine appear different. In particular, the thymine C4=O band at 1660 cm⁻¹ shows smaller enhancement upon interaction. This indicates that the different stereochemistry of the side-chain promotes different interactions of **21** with the bases in the loops, which could correlate with the unusually high emission enhancement of **21** upon c-myc binding.

In order to quantify the intensity changes observed upon interaction of the Pt-complexes with c-myc, the UVR spectra were deconvoluted using Voigt functions (e.g., see Supporting Information, Figure S55) and the peak areas were compared. The intensity changes are illustrated in Figure 6, where the percentage change in the intensity of specific peaks, corresponding to certain bases in the quadruplex, is compared for each complex as a measure of the extent of its interaction with c-myc. The percentage changes were calculated using Equation (1):

$$\text{Change (\%)} = \frac{(\text{Area}(\text{Pt-complex}) - \text{Area}(\text{c-myc}))}{\text{Area}(\text{c-myc})} * 100 \quad (1)$$

For each base, representative band(s) were selected, which were those at 1320/1337, 1580/1610, and ~1660 cm⁻¹ for adenine, guanine and thymine, respectively (Figure 5B). It is important to note that this approach emphasizes only intensity changes in the particular bands chosen and does not necessarily portray the totality of the interactions between the Pt-complex and the DNA. Figure 6 shows that all Pt-complexes significantly modify the guanine-quartet environment, and

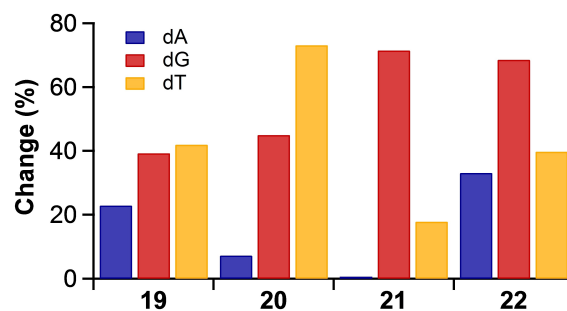


Figure 6. Graphical illustration of quantification of structural changes induced by each Pt-complex at the different bases present in c-myc. The representative peaks for adenine are 1320 and 1337 cm⁻¹ (blue); for guanine 1580 and 1610 cm⁻¹ (red); and for thymine 1660 cm⁻¹ (yellow).

interact to a different extent with the residues in the G-quadruplex loops. For example, complex **20** shows increased interactions with the thymine and less with adenine. Interestingly, the two enantiomers **21** and **22** show similar interactions with the guanines, however, the L-isomer shows diminished interactions with thymines and adenines in the loops, which we attribute to the different stereochemistry of the side-chains. The docking simulations described below confirm this variation in the interactions and help shed light to the positioning of each Pt-complex at the terminus of the G-quadruplex stack.

It should be noted that the interactions of Pt-complexes **19–22** with hybrid telomeric G-quadruplex (22AG/K⁺) were also investigated by Resonance Raman (see Supporting Information), which indicated differential behaviour among the various side chains, including those of the two enantiomers **21** and **22**, with noticeable effects involving G-quartet guanines, as well as loop thymines and adenines. Despite the modest association of all complexes with 22AG/K⁺, compared to c-myc, as determined by UV-vis and fluorescence titrations, this 22AG/K⁺ structure appears susceptible to conformational changes. This is evident in both UVRR (Supporting Information, Figures S56–57) as well as CD spectra (Supporting Information, Figure S49) of the DNA mixtures with the investigated Pt-complexes.

Finally, the (low affinity) interactions of a representative Pt-compound, **22**, with antiparallel telomeric G-quadruplex (22AG/Na⁺) and duplex (ds26) DNA corresponded to only minor changes in the RR spectra (Supporting Information, Figure S59).

Docking simulations of interactions between Pt(II)-complexes and c-myc

For each of the four optimal Pt-complexes, **19–22**, an ensemble docking protocol was performed and repeated five times (see computational details in the Experimental Section) on the 20 c-myc G-quadruplex conformers issued from NMR coordinates (PDB ID: 1XAV). The best affinity scores, as well as the G-quadruplex conformers related to the docking solutions, the number of close contacts and a list of interactions with the G-quadruplex residues are summarized in Supporting Information, Table S7.

Among the four Pt-complexes examined, compound **20** shows the best affinity score (−9.3 kcal.mol^{−1}), in agreement with the highest K_s from UV-vis and fluorescence titrations and the highest ΔT_m from the DNA melting experiment. The highest number of close contacts with the c-myc G-quadruplex target is also observed with compound **20** (>40 close contacts at a distance below 3.5 Å), indicating that **20** is deeply docked into c-myc (Figure 7A). For the five docking runs, the best docking solution of **20** was always obtained with conformer #8 (Supporting Information, Figure S62), for which the distance between the first thymine (T1) and the first G-tetrad is the lowest (Supporting Information, Figure S60). Additionally, conformer #8 is the only one for which the sugar-base dihedral angle of T1 is *syn* (−90°) while the corresponding dihedral angle is *anti* for the 19 other conformers (Supporting Information, Table S8). Therefore, the T1 base is close to the first

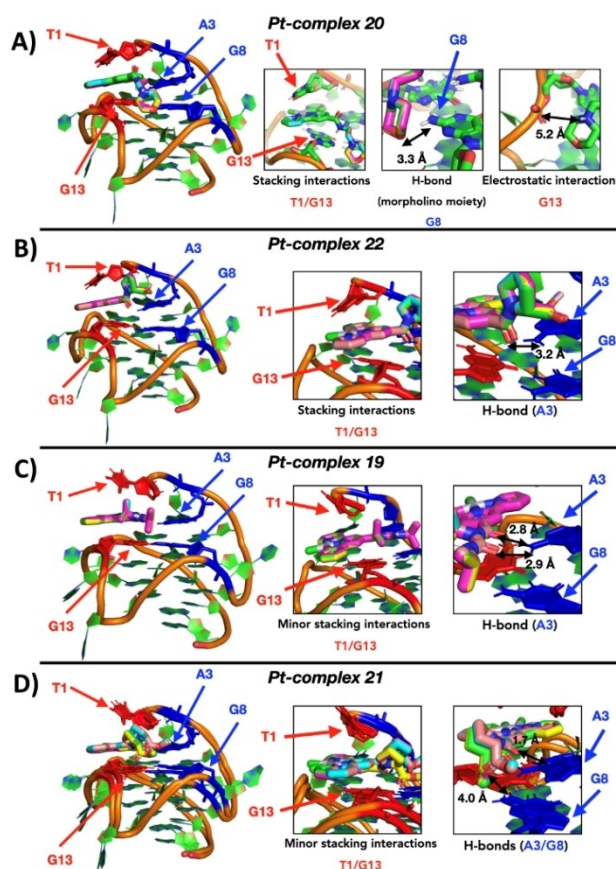


Figure 7. Superposition of the best binding modes between each ligand and c-myc G-quadruplex. Selected residues are represented in red sticks (T1/G13) or blue sticks (A3/G8). G-quadruplex conformers are represented in cartoon mode. For each Pt-complex, the main interactions encountered in the best binding modes are zoomed on the right.

G-tetrad plane and oriented in such a way that the aromatic moieties of T1 and G13 form a narrow pocket in which the aromatic core of **20** can be docked via end-stacking interaction. We observed that, for the five docking runs of **20**, from a total of >40 close contacts between **20** and the G-quadruplex target (Supporting Information, Table S7), 25 of them turn out to be close contacts with either G13 (14 close contacts) or T1 (11 close contacts). The other close contacts are owing to the interactions between the morpholino fragment and G8, as one H-bond is formed between the oxygen atom of the morpholino group and the G8 amino group (Figure 7A). Interestingly, the positive charge of the morpholino group is also closely positioned to the phosphate of G13, assisting the H-bond with an electrostatic interaction (Figure 7A). Such a deep positioning of the morpholino group into the closed G-quadruplex conformer is allowed thanks to the use of a flexible linker between the aromatic and morpholino moieties of **20**.

For Pt-complex **22**, the best docking solutions were also obtained with the G-quadruplex conformer #8 (Supporting Information, Figure S63). The aromatic core of **22** is also docked between the residues T1 and G13 (Figure 7B). However, the aromatic moieties of **22** are closer to T1 (15 close contacts) than

G13 (7 close contacts), an opposite situation compared to the case of compound **20** (Supporting Information, Table S7). With a peripheral side-chain in **22** that is shorter, bulkier and more rigid than the linker of **20**, we observed a different docking in the upper region of the G-quadruplex target, showing the formation of one H-bond with the amino group of A3 residue (Figure 7B). This H-bond involves the oxygen atom of the imide, located in proximity of the aromatic core of the Pt-complex. The rigidity and the orientation of the proline group, guided by a specific stereochemistry (D-enantiomer), forced the ligand to be docked in the upper region of the G-quadruplex target, with the terminal chain of the ligand exposed to the solvent environment (Figure 7B). This is in contrast with **20**, for which the morpholino group was deeply docked around the first G-tetrad. The affinity of **22** is lower in comparison to **20**, but remains relatively high ($-8.8 \text{ kcal.mol}^{-1}$) due to the efficient stacking and H-bonding interactions.

For Pt-complex **19**, the best docking solutions were obtained with G-quadruplex conformer #16 (Supporting Information, Figure S64), a more 'open' structure in terms of distance between the plane formed by the first G-tetrad and the T1 residue (Supporting Information, Figure S61, left). Additionally, the orientation of the T1 residue is rather different as the sugar-base dihedral angle of T1 is *anti* (-158°) whereas the corresponding dihedral angle was *syn* in conformer #8 (Supporting Information, Table S8). The preference of **19** for such an 'open' conformer can be explained by the bulkiness of its side-chain and especially the presence of two isopropyl fragments connected to the two nitrogen atoms. Moreover, the carbamoyl amide fragment allows the formation of two H-bonds with residue A3 (Figure 7C). While the binding modes of both **20** and **22** were guided by strong end-stacking interactions within the 'closed' target conformer #8, the binding of **19** is mainly guided by H-bonding in the upper region of the G-quadruplex target (A3 residue). At the same time, stacking interactions are clearly less efficient, with a low number of close contacts involving the G13 and no contacts with T1 (Supporting Information, Table S7). Nevertheless, the aromatic groups of **19** are still positioned between the T1 and G13 residues (Figure 7C), but the stacking interactions are much less optimized because of the higher degree of opening in this c-myc conformer. Therefore, Pt-complex **19** exhibits the lowest number of close contacts, i.e., only 13 to 18 contacts (Supporting Information, Table S7). The affinity score of **19** is lower than the one of **20**, but still at $-8.8 \text{ kcal.mol}^{-1}$ (as for **22**) thanks to the two strong H-bonds involving the oxygen atoms of the side-chain.

For Pt-complex **21**, the enantiomer of **22**, the best docking solutions were also obtained with 'open' target conformers, i.e., two with conformer #16 and three with conformer #20 (Supporting Information, Figures S65,61). In this case, two H-bonds are observed between the amino groups of two different residues, i.e., A3 and G8 (Figure 7D). In comparison to **19**, complex **21** is found closer to the A3 and G8 residues (more close contacts), but there are no close contacts with G13 (Supporting Information, Table S7). Therefore, Pt-complex **21** is the least efficient in terms of end-stacking interactions involving

the T1 and G13 residues, but the most efficient ligand in terms of H-bonding as it involves two different residues. The affinity score of **21** is comparable to the affinity scores of **19** or **22** (Supporting Information, Table S7), whereas the binding modes are quite different.

Conclusions

The current study delivered, through a robust synthesis, a new class of DNA-interacting agents, based on the square planar (2-([2,2'-bipyridin]-6-yl)phenyl)platinum(II) scaffold, for in vitro evaluation of their efficiency in binding topologically diverse DNA secondary structures, including the c-myc oncogene promoter G-quadruplex, the 22AG (telomeric) hybrid and parallel G-quadruplexes, duplex ds26 and ssDNA polyT. Our intention was to evolve this stable, planar organometallic scaffold with additional moieties, that would ideally enhance its affinity and recognition selectivity in favour of G-quadruplex targets.

In the design of these organometallic compounds, emphasis was placed on the selection of appendages added to the main scaffold, aiming to mimic specific structural features of G-quadruplex-recognizing peptides that impact the nature of interaction, either electronically or sterically.^[40] These involved bulky lipophilic or heteroaryl side chains, ionizable amino-residues, hydrogen-bonding moieties and chiral groups. The individual contributions to binding affinity and G-quadruplex stabilization of several of these attributes is often side-stepped in studies of conventional charged Pt-complex binders, most of which lack such elaborate appendage design, while their presence in organometallic counterparts has not been systematically investigated.

The synthesized Pt(II)-compounds exhibited binding selectivity toward c-myc, and to a lesser extent 22AG (both folds tested), with only weak affinity for ds26 and no affinity for polyT. Importantly, these compounds behave as potent binders for c-myc, with K_a values in the order of 10^5 M^{-1} , as determined by two independent methods, UV-vis titrations and fluorescence titrations. Their K_a values compare well with those of related charged Pt-terpyridine complexes, suggesting that the presence of the proposed appendages counteracts the absence of a charged scaffold in our compounds, likely by contributing interactions with G-quadruplex loci other than G-tetrads, in addition to the end-stacking interaction of the planar organometallic scaffold.

A remarkable feature is the stabilizing effects of this class of G-quadruplex binders on c-myc, with the ΔT_m value for the optimal binder (**20**) exceeding 30°C , which renders it superior to many known metal-based binders. Moreover, even the weakest binder, a neutral Pt-complex with rigid heteroaromatic side-chain (**23**), appeared to be a potent stabilizer of c-myc. Notably, the CD-based melting experiment for ΔT_m determination suggested, by means of a bimodal sigmoidal curve, combined stabilizing effects on the G-tetrad core and loop elements of the c-myc G-quadruplex, by the organoplatinum scaffold and appendages, respectively.

Gratifyingly, representatives of this compound class (in particular compound **21**) undergo remarkable emission enhancements upon their interaction with c-myc, which are several times higher compared to those observed with all other DNAs included in the study. Therefore, compounds like **21** may be employed as selective c-myc-targeted optical probes.

UV Resonance Raman measurements involving the four most promising compounds (**19–22**), with regard to their affinity and optical properties, confirmed that they cause stabilization of the c-myc G-quadruplex, providing direct evidence for the specific interactions at work. All complexes demonstrate modification of the guanine environment suggesting π - π stacking with the outer G-tetrads. However, the different side chains promote varied interactions with the loop residues, which are responsible for the different association constants and ΔT_m values observed in the UV-vis and fluorescence titrations and CD melting experiment, respectively. Complex **20** shows increased interaction with the thymine in the loops but not adenine, as does the D-proline enantiomer **22**, in contrast to its L-isomer **21**, which also shows diminished interaction with adenine, suggesting a role for stereochemistry in the stabilization of the helix.

The above results are supported by docking simulations, showing that the nature, the length, the stereochemistry and the bulkiness of the appendage impact the binding mode of the Pt-complexes with the c-myc G-quadruplex target. The rather long and flexible linker of **20** allows optimal stacking interactions (T1/G13) on a 'closed' G-quadruplex conformer along with one optimal H-bond with a deeply-located residue. With a rigid and bulkier side-chain, **19** is preferably docked with an 'open' G4 conformation. Stacking interactions are less optimal but the affinity score remains high thanks to the introduction of H-bond acceptor moieties (carbamoyl amide group) that lead to two optimum H-bonds with a residue in the loop (A3). Interestingly, the enantiomers **21** and **22** exhibit different binding modes which, in agreement with the UVRR results, highlights the importance of the stereochemistry of the Pt-complex side-chains on c-myc G-quadruplex binding.

In summary, the current study shines light into various aspects relevant to the impact of peptide-mimetic side-chains in G-quadruplex target interaction and affinity, recognition selectivity and stabilization, as well as optical response of the binder itself. These findings may help inform next-generation metal-based G-quadruplex binder design, aiming toward elevated selectivity in G-quadruplex target recognition. The neutral organometallic scaffold employed herein proved to be a viable recognition motif for c-myc, among the DNAs tested, efficient both as stabilizer and optical probe. It is further hoped that it will help address issues of chemical stability of Pt-complexes, cell membrane permeability, toxicity regulation and target optical detection. We intend to investigate the plausibility of this hypothesis in follow-up cell-based studies.

Experimental Section

Compound synthesis, purification and characterization: Organic chemicals were purchased from TCI Europe N.V., platinum salts from Strem Chemicals, other inorganic chemicals from Sigma-Aldrich, anhydrous organic solvents from Carlo Erba Reagents, silica gel 60, TLC plates and NMR deuterated solvents from Merck.

All reactions were performed under nitrogen atmosphere and in anhydrous solvents, unless otherwise stated. Reaction progress was monitored by TLC. Silica gel 60 (0.06–0.2 mm) was employed in liquid chromatography purifications of organic intermediates.

NMR spectra were obtained on a Bruker Avance III Ultrashield Plus spectrometer (at 500 MHz for ^1H NMR and 125 MHz for ^{13}C NMR, at 25 °C, chemical shifts relative to tetramethylsilane). MS data were collected on a Bruker Autoflex III Smartbeam MALDI-TOF/TOF instrument, using a MTP384 ground steel plate.

Detailed synthetic and purification procedures for all compounds synthesized in this study, as well as characterization data and original NMR spectra are provided in the Supporting Information.

Single-crystal X-ray diffraction (XRD): Single crystal X-ray diffraction data were collected on an Oxford Diffraction Supernova diffractometer, equipped with a CCD area detector utilizing Mo–K α ($\lambda=0.71073$ Å) radiation. Suitable crystals of compound **19** were attached to glass fibers using paratone-N oil and transferred to a goniostat where they were cooled for data collection. Empirical absorption corrections (multi-scan based on symmetry-related measurements) were applied using CrysAlis RED software (Oxford Diffraction Ltd, Abingdon, Oxford, England, 2008). The structures were solved by direct methods with SHELXT and refined on F2 using full-matrix least squares with SHELXL-2014/7 (G. M. Sheldrick, University of Göttingen, Germany, 2014). Software packages CrysAlis CCD for data collection and CrysAlis RED for cell refinement and data reduction (Oxford Diffraction Ltd, Abingdon, Oxford, England, 2008), WINGX for geometric calculations,^[62] and MERCURY^[63] for molecular graphics, were used. The non-hydrogen atoms were treated anisotropically, whereas the hydrogen atoms were placed in calculated, ideal positions and refined as riding on their respective carbon atoms. Selected crystal data and crystallographic analysis details for compound **19** can be found in Supporting Information (Tables S1–5).

CCDC 2095012 (**19**) contains the supplementary crystallographic data for this paper. These data are provided free of charge by The Cambridge Crystallographic Data Centre.

UV-vis titrations of Pt(II)-complexes with DNAs: Oligonucleotides c-myc (myc2345–pu22, 5'-TGAGGGTGGGTAGGGTGGGTAA-3'), 22AG (5'-AGGGTTAGGGTTAGGGTTAGGG-3') and ds26 (5'-CAATCGGATC-GAATTCGATCCGATTG-3') were purchased from Eurogentec (Belgium) and polyT (dT₂₀) was purchased from Sigma-Aldrich. Each DNA was dissolved in 50 mM Tris.HCl buffer (pH 7.4) containing 100 mM KCl or NaCl, to afford a concentrated solution (0.57–2.15 M). The following solutions were prepared: c-myc/K⁺, 22AG/K⁺, 22AG/Na⁺, ds26/K⁺, polyT/K⁺. Prior to use, each concentrated DNA solution (except polyT) was annealed at 95 °C for 5 min, followed by slow cooling to r.t. overnight. The concentration was then confirmed by UV-vis, based on the extinction coefficient values provided by the suppliers.

A stock solution of each Pt-complex was prepared in DMSO at 3 mM concentration. In a 10 mm optical path quartz cuvette, 25 μL of Pt-complex stock solution were diluted with 50 mM Tris.HCl buffer (pH 7.4) containing 100 mM KCl or NaCl, up to a final volume of 2.5 mL, affording a 30 μM work solution (1% v/v in DMSO content). The UV-vis spectrum of this work solution, in the range

200–600 nm, was recorded on a Shimadzu UV-1700 Pharmaspec UV-Vis spectrophotometer. A titration was carried out by adding 2.5 μL aliquots of the concentrated pre-folded DNA solution to the cuvette and mixing thoroughly for 5 mins, before recording the new spectrum.

The absorbance at the selected maximum in the course of the titration was plotted vs. total added DNA concentration, corrected for the dilution factor. A non-linear model (growth sigmoidal function, Hill1 equation, Levenberg-Marquardt iteration algorithm) was direct-fitted to the data in ORIGIN Pro, leading to determination of association constants (K_a) and number of cooperative sites (n) for the Pt-complex-DNA interaction.

Fluorescence titrations of Pt(II)-complexes with DNAs: A 10 mM Li-cacodylate aqueous buffer (pH 7.2) containing either KCl or NaCl at 100 mM concentration was used for preparing 100 μM DNA work solutions (c-myc/ K^+ , 22AG/ K^+ , 22AG/ Na^+ , ds26/ K^+ , polyT/ K^+). Each buffered DNA work solution was annealed at 95 $^\circ\text{C}$ for 5 min, then allowed to cool slowly at r.t. overnight.

Pt-complexes were employed as 2 mM work solutions in DMSO. Thirteen mixtures representing various DNA-to-Pt-complex molar ratios in the titration (0, 0.25, 0.5, 0.75, 1, 1.5, 2, 2.5, 3, 3.5, 4, 4.5, 5) were prepared, by combining appropriate volumes of Pt-complex and DNA work solutions with additional buffer, all to the same final volume and to a fixed final concentration of the tested Pt-complex (5 μM), but variable final concentration of DNA (DMSO was kept at 0.25% v/v). Mixtures were gently agitated in Eppendorf tubes for 5 min. The emission spectrum of each mixture was recorded on a Jasco FP-6300 spectrofluorometer. All spectra were obtained at 21 $^\circ\text{C}$ by using a high-precision quartz suprasil cuvette (light path 10 mm \times 0.5 mm). Excitation took place at 320 nm and emission spectra were recorded in the 350–800 nm range, with the following parameters: 5 nm bandwidth (exc.), 10 nm bandwidth (em.), high response, high sensitivity, 1 nm data pitch, 500 nm.min⁻¹ scanning speed, and 3 accumulations. Baseline correction was made to all spectra by subtracting the spectrum of the buffer, containing the same percentage of DMSO as the mixtures.

The maximum fluorescence (I) of each mixture from the emission band was normalized by dividing with the emission maximum of the free Pt-compound in the absence of DNA (I_0). Normalized fluorescence maxima (norm. max. fluorescence, I/I_0) were plotted vs. total added DNA concentration and the data was fitted with a non-linear model (growth-sigmoidal function, Hill1 equation, Levenberg-Marquardt iteration algorithm, fixed starting point) in ORIGIN Pro, which allowed determination of association constant (K_a) and number of cooperative sites (n) for the Pt-complex-DNA interaction. The last and first spectrum of each titration (5 and 0 equiv. of DNA, respectively, relative to Pt-complex), were used to derive emission enhancements, calculated as the ratio of the two maxima.

Circular dichroism DNA-melting study: The oligonucleotide c-myc was dissolved in MilliQ water to afford a 1 mM stock solution. This solution was then diluted with 10 mM Li-cacodylate buffer (pH 7.2) containing KCl at 1 mM concentration and LiCl at 99 mM concentration, to produce a 10 μM DNA work solution. Prior to use, the work solution was annealed at 95 $^\circ\text{C}$ for 5 min, followed by cooling in an ice bath for 1 h. Pt-complex 50 μM work solutions in the same buffer were used (1% v/v in DMSO). Equal volumes of DNA and Pt-complex work solutions were mixed to produce a mixture containing 1:5 molar ratio of DNA-to-ligand (final concentrations: 5 μM and 25 μM , respectively).

CD spectra were recorded on a Chirascan™ Plus CD spectrophotometer from Applied Photophysics, equipped with a TC125 temperature controller from Quantum Northwestern. CD meas-

urements were performed, in the range 220–320 nm, using a response time of 1 s, 1 nm step, and 0.5 nm bandwidth. Each spectrum was recorded 3 times of which the normalized average is presented, with the spectrum of the buffer subtracted from that of the sample. For melting experiments, the solution (pure oligonucleotide or oligonucleotide plus Pt-complex) was placed in a quartz cuvette, heated from a baseline temperature of 20 $^\circ\text{C}$ to 95 $^\circ\text{C}$, at the rate of 1 $^\circ\text{C}$ per minute, and CD spectra were recorded at intervals of 5 $^\circ\text{C}$.

Melting curves were obtained by plotting normalized molar ellipticity based on the 265 nm positive peak vs. temperature in ORIGIN Pro and fitting a non-linear model (sigmoidal function, BiDose response, Levenberg-Marquardt iteration algorithm).

UV resonance Raman study: Pt-complexes 19–22 were initially dissolved in DMSO and then diluted in 50 mM Tris.HCl buffer (pH 7.4) containing 100 mM KCl to prepare stock solutions with concentration 375 μM . A 67.5 μM stock solution of c-myc was also prepared by dissolving c-myc oligonucleotide in the same buffer. The c-myc stock solution was annealed at 95 $^\circ\text{C}$ for 5 mins, followed by cooling in an ice bath for 1 h immediately prior to use. Appropriate volumes of Pt-complex and c-myc stock solutions were mixed to produce a solution with final concentrations of 178 μM and 35.5 μM for Pt-complex and c-myc, respectively (5:1 molar ratio), which was used for UVRr experiments.

Resonance Raman experiments were conducted with excitation at 266 nm provided by the fourth harmonic of a Q-switched Nd:YAG laser (PRO-230, 30 Hz, Spectra Physics). The excitation light was focused into a spinning cell consisting of an EPR suprasil tube (4 mm diameter) attached to a rheostat-controlled motor for choice of rotation speed. Use of the spinning cell prolonged the lifetime of the samples. Modest excitation energies (3.3 μJ per pulse) were employed to avoid decomposition of the sample, which was monitored by obtaining the absorption spectrum of the sample before and after exposure. The Raman scattered light was collected in a backscattering geometry and delivered to a 0.75 m focal-length Czerny-Turner spectrograph, equipped with a 2400 grooves/mm holographic grating. The slit width was set to 100 μm providing 7 cm^{-1} spectral resolution at 266 nm. The scattered light was detected by a LN₂-cooled 2048 \times 512 pixel, back-illuminated UV-enhanced CCD detector (Spec10:2KBUV/LN, Princeton Instruments). Each spectrum with excitation at 266 nm is the accumulation of 20 \times 10 min spectra. Frequency calibration of the spectra was accomplished with the use of cyclohexane. MATLAB and ORIGIN software were used for spectral treatment and analysis.

Docking simulation methods: Pt-complexes 19–22 were built within the Avogadro molecular editor.^[64] The 3D coordinates of the crystal structure shown in Figure 1 were used as a starting template, and the correct side-chain was replaced for each Pt-complex, using the Avogadro package. Molecular mechanics calculations were then performed within Avogadro to optimize the geometry of the four Pt-complexes. For this, a steepest descent optimization (10,000 steps) was performed with the Universal Force Field (UFF)^[65] to consider the platinum parameters. The energy convergence criterion was set at 10⁻⁷ kJ.mol⁻¹ for the energy minimization procedure. The coordinates of the c-myc G-quadruplex were obtained from the Protein Data Bank (PDB ID: 1XAV).^[66] The NMR conformations of the G-quadruplex were extracted to perform ensemble docking calculations, i.e., twenty conformers for the 1XAV coordinates, to take account in an implicit way of the target flexibility. Docking calculations were performed with the QuickVina-W package,^[67] a fork of AutoDock Vina package,^[68] optimized for wide search space and blind docking. Since the Pt atom types are not explicitly included in these packages, the source

code was modified to consider explicitly Pt atoms. Pt atom type as well as its parameters were included, i.e. atomic radius (1.375 Å), van der Waals well depth (0.080 kcal.mol⁻¹), atomic solvation parameter (−0.00110, similar to other metal atoms in the Autodock energy parameters), atomic solvation volume (12.00 Å³), and the covalent radius (1.28 Å). The source code was then recompiled to allow the explicit treatment of the Pt atom. Given the lack of knowledge concerning the binding modes of the four Pt-ligands, a sufficiently large grid was needed to perform blind docking calculations for the exploration of the entire G-quadruplex surface. Therefore, a large grid size of 42×36×42 Å³ with a spacing of 1.0 Å was considered. The center of the grid box was located on the center-of-mass of the G-quadruplex targets. Due to the important size of the grids, a large exhaustiveness value of 64 was chosen, much larger than the default value, i.e., 8.^[69] The four Pt-ligands were set as flexible entities with flexibility on torsions along the linker of the ligands. The 10 most energetically favorable complexes were retained for each docking calculation. The docking protocol was repeated 5 times to ensure the reproducibility of the optimum docking solutions. The PyMOL molecular visualization system was used to depict illustrations of the docking binding modes (W. L. Delano, Delano Scientific, San Carlos, 2002).

Acknowledgements

S.N.G. and S.C.H. acknowledge the University of Cyprus for funding of this project and for contributing open access publication fees for this article. S.N.G. would like to thank Prof. E. Pinakoulaki and Prof. N. Chronakis (Dept. of Chemistry, UCY) for providing access to UV-vis and CD spectrophotometers, respectively, as well as Prof. A. Kirmizis (Dept. of Biological Sciences, UCY) and his team members for assistance with denaturing urea PAGE. S.C.H. would like to thank E. Mitrakou for help with the UVRF experiments on 22AG/K⁺. Research in Mons (M.S.) is supported by the University of Mons, the Wallonia Region and the Fund for Scientific Research (F.R.S.-FNRS) under the grant EOS No. 30650939 (PRECISION).

Conflict of Interest

The authors declare no conflict of interest.

Data Availability Statement

The data that support the findings of this study are available in the supplementary material of this article.

Keywords: c-myc · docking simulation · emission enhancement · end-stacking · G-quadruplexes · organoplatinum compounds · resonance Raman

- [1] a) A. M. Zahler, J. R. Williamson, T. R. Cech, D. M. Prescott, *Nature* **1991**, 350, 718–720; b) A. L. Moye, K. C. Porter, S. B. Cohen, T. Phan, K. G. Zyner, N. Sasaki, G. O. Lovrecz, J. L. Beck, T. M. Bryan, *Nat. Commun.* **2015**, 6, 7643; c) M.-L. Zhang, X.-J. Tong, X.-H. Fu, B. O. Zhou, J. Wang, X.-H. Liao, Q.-J. Li, N. Shen, J. Ding, J.-Q. Zhou, *Nat. Struct. Mol. Biol.* **2010**, 17, 202–209.

- [2] a) Y. Hou, F. Li, R. Zhang, S. Li, H. Liu, Z. S. Qin, X. Sun, *Epigenetics* **2019**, 14, 894–911; b) H. Hegyi, *Sci. Rep.* **2015**, 5, 9165.
- [3] a) S.-Q. Mao, A. T. Ghanbarian, J. Spiegel, S. M. Questa, D. Beraldi, M. Di Antonio, G. Marsico, R. Hänsel-Hertsch, D. Tannahill, S. Balasubramanian, *Nat. Struct. Mol. Biol.* **2018**, 25, 951–957; b) P. Sarkies, C. Reams, L. J. Simpson, J. E. Sale, *Mol. Cell* **2010**, 40, 703–713; c) G. Guilbaud, P. Murat, B. Recolin, B. C. Campbell, A. Maiter, J. E. Sale, S. Balasubramanian, *Nat. Chem.* **2017**, 9, 1110–1117.
- [4] a) N. Puget, K. M. Miller, G. Legube, *DNA Repair* **2019**, 81, 102661; b) I. Georgakopoulos-Soares, S. Morganello, N. Jain, M. Hemberg, S. Nik-Zainal, *Genome Res.* **2018**, 28, 1264–1271; c) E. Kruissebrink, V. Guryev, K. Brouwer, D. B. Pontier, E. Cuppen, M. Tijsterman, *Curr. Biol.* **2008**, 18, 900–905; d) K. Paeschke, M. L. Bochman, P. D. Garcia, P. Cejka, K. L. Friedman, S. C. Kowalczykowski, V. A. Zakian, *Nature* **2013**, 497, 458–462.
- [5] a) A.-L. Valton, M.-N. Prioleau, *Trends Genet.* **2016**, 32, 697–706; b) H. Técher, S. Koundrioukoff, A. Nicolas, M. Debatisse, *Nat. Rev. Genet.* **2017**, 18, 535–550.
- [6] a) J. L. Huppert, S. Balasubramanian, *Nucleic Acids Res.* **2007**, 35, 406–413; b) T. Simonsson, P. Penicka, M. Kubista, *Nucleic Acids Res.* **1998**, 26, 1167–1172; c) R. Hänsel-Hertsch, D. Beraldi, S. V. Lensing, G. Marsico, K. Zyner, A. Parry, M. Di Antonio, J. Pike, H. Kimura, M. Narita, D. Tannahill, S. Balasubramanian, *Nat. Genet.* **2016**, 48, 1267–1272.
- [7] a) R. Shahid, A. Bugaut, S. Balasubramanian, *Biochemistry* **2010**, 49, 8300–8306; b) S. Lammich, F. Kamp, J. Wagner, B. Nuscher, S. Zilow, A.-K. Ludwig, M. Willem, C. Haass, *J. Biol. Chem.* **2011**, 286, 45063–45072; c) P. Agarwala, S. Pandey, K. Mapa, S. Maiti, *Biochemistry* **2013**, 52, 1528–1538.
- [8] a) J. Spiegel, S. Adhikari, S. Balasubramanian, *Trends Chem.* **2020**, 2, 123–136; b) M. L. Bochman, K. Paeschke, V. A. Zakian, *Nat. Rev. Genet.* **2012**, 13, 770–780.
- [9] a) J. Dai, M. Carver, D. Yang, *Biochimie* **2009**, 90, 1172–1183; b) D. Bhattacharyya, G. M. Arachchilage, S. Basu, *Front. Chem.* **2016**, 4, 38.
- [10] K. Paeschke, T. Simonsson, J. Postberg, D. Rhodes, H. J. Lipps, *Nat. Struct. Mol. Biol.* **2005**, 12, 847–854.
- [11] a) N. Kumar, S. Maiti, *Nucleic Acids Res.* **2008**, 36, 5610–5622; b) A. N. Lane, J. B. Chaires, R. D. Gray, J. O. Trent, *Nucleic Acids Res.* **2008**, 36, 5482–5515.
- [12] H. J. Lipps, D. Rhodes, *Trends Cell Biol.* **2009**, 19, 414–422.
- [13] a) C. Schaffitzel, I. Berger, J. Postberg, J. Hanes, H. J. Lipps, A. Plückthun, *Proc. Natl. Acad. Sci. USA* **2001**, 98, 8572–8577; b) G. Biffi, D. Tannahill, J. McCafferty, S. Balasubramanian, *Nat. Chem.* **2013**, 5, 182–186; c) A. Henderson, Y. Wu, Y. C. Huang, E. A. Chavez, J. Platt, F. B. Johnson, R. M. Brosh, Jr, D. Sen, P. M. Lansdorp, *Nucleic Acids Res.* **2014**, 42, 860–869; d) G. Biffi, D. Tannahill, J. Miller, W. J. Howat, S. Balasubramanian, *PLoS One* **2014**, 9, e102711.
- [14] a) A. Laguerre, K. Hukezalie, P. Winckler, F. Katranji, G. Chanteloup, M. Pirrotta, J.-M. Perrier-Cornet, J. M. Y. Wong, D. Monchaud, *J. Am. Chem. Soc.* **2014**, 136, 12406–12414; b) A. Shivalingam, M. A. Izquierdo, A. Le Marois, A. Vyšniauskas, K. Suhling, M. K. Kuimova, R. Vilar, *Nat. Commun.* **2015**, 6, 8178; c) C.-C. Chang, J.-Y. Wu, T.-C. Chang, *J. Chin. Chem. Soc.* **2003**, 50, 185–188; d) Q. Yang, J. Xiang, S. Yang, Q. Zhou, Q. Li, Y. Tang, G. Xu, *Chem. Commun.* **2009**, 1103–1105; e) Y.-J. Lu, D.-P. Hu, K. Zhang, W.-L. Wong, C.-F. Chow, *Biosens. Bioelectron.* **2016**, 81, 373–381; f) S. Zhang, H. Sun, L. Wang, Y. Liu, H. Chen, Q. Li, A. Guan, M. Liu, Y. Tang, *Nucleic Acids Res.* **2018**, 46, 7522–7532.
- [15] For a review, see: L. Savva, S. N. Georgiades, *Molecules* **2021**, 26, 841.
- [16] a) A. Siddiqui-Jain, C. L. Grand, D. J. Bearss, L. H. Hurley, *Proc. Natl. Acad. Sci. USA* **2002**, 99, 11593–11598; b) S. Cogo, L. E. Xodo, *Nucleic Acids Res.* **2006**, 34, 2536–2549; c) M. Bejugam, S. Sewitz, P. S. Shirude, R. Rodriguez, R. Shahid, S. Balasubramanian, *J. Am. Chem. Soc.* **2007**, 129, 12926–12927; d) J. Amato, A. Pagano, D. Capasso, S. Di Gaetano, M. Giustiniano, E. Novellino, A. Randazzo, B. Pagano, *ChemMedChem* **2018**, 13, 406–410; e) Y. Wu, L.-P. Zan, X.-D. Wang, Y.-J. Lu, T.-M. Ou, J. Lin, Z.-S. Huang, L.-Q. Gu, *Biochim. Biophys. Acta Gen. Subj.* **2014**, 1840, 2970–2977.
- [17] a) D. Drygin, A. Siddiqui-Jain, S. O'Brien, M. Schwaebe, A. Lin, J. Bliesath, C. B. Ho, C. Proffitt, K. Trent, J. P. Whitten, J. K. C. Lim, D. Von Hoff, K. Anderes, W. G. Rice, *Cancer Res.* **2009**, 69, 7653–7661; b) H. Xu, M. Di Antonio, S. McKinney, V. Mathew, B. Ho, N. J. O'Neil, N. Dos Santos, J. Silvester, V. Wei, J. Garcia, F. Kabeer, D. Lai, P. Soriano, J. Banáth, D. S. Chiu, D. Yap, D. D. Le, F. B. Ye, A. Zhang, K. Thu, J. Soong, S.-C. Lin, A. H. C. Tsai, T. Osako, T. Algara, D. N. Saunders, J. Wong, J. Xian, M. B. Bally, J. D. Brenton, G. W. Brown, S. P. Shah, D. Cescon, T. W. Mak, C.

- Caldas, P. C. Stirling, P. Hieter, S. Balasubramanian, S. Aparicio, *Nat. Commun.* **2017**, *8*, 14432.
- [18] a) G. Zhou, X. Liu, Y. Li, S. Xu, C. Ma, X. Wu, Y. Cheng, Z. Yu, G. Zhao, Y. Chen, *Oncotarget* **2016**, *7*, 14925–14939; b) T. Che, S.-B. Chen, J.-L. Tu, B. Wang, Y.-Q. Wang, Y. Zhang, H. Wang, Z.-Q. Zhang, Z.-P. Zhang, T.-M. Ou, Y. Zhao, J.-H. Tan, Z.-S. Huang, *J. Med. Chem.* **2018**, *61*, 3436–3453; c) F. Berardinelli, M. Tanori, D. Muoio, M. Buccarelli, A. di Masi, S. Leone, L. Ricci-Vitiani, R. Pallini, M. Mancuso, A. Antocchia, *J. Exp. Clin. Cancer Res.* **2019**, *38*, 311; d) M.-H. Hu, S.-B. Chen, B. Wang, T.-M. Ou, L.-Q. Gu, J.-H. Tan, Z.-S. Huang, *Nucleic Acids Res.* **2017**, *45*, 1606–1618.
- [19] a) G. Miglietta, S. Cogoi, J. Marinello, G. Capranico, A. S. Tikhomirov, A. Shchekotikhin, L. E. Xodo, *J. Med. Chem.* **2017**, *60*, 9448–9461; b) Y. Katsuda, S.-I. Sato, L. Asano, Y. Morimura, T. Furuta, H. Sugiyama, M. Hagihara, M. Uesugi, *J. Am. Chem. Soc.* **2016**, *138*, 9037–9040.
- [20] D. Yang, K. Okamoto, *Future Med. Chem.* **2010**, *2*, 619–646.
- [21] P. Chilka, N. Desai, B. Datta, *Molecules* **2019**, *24*, 752.
- [22] a) S. Asamitsu, T. Bando, H. Sugiyama, *Chem. Eur. J.* **2019**, *25*, 417–430; b) M. P. O' Hagan, J. C. Morales, M. C. Galan, *Eur. J. Org. Chem.* **2019**, 2019, 4995–5017.
- [23] a) S. N. Georgiades, N. H. Abd Karim, K. Suntharalingam, R. Vilar, *Angew. Chem. Int. Ed.* **2010**, *49*, 4020–4034; *Angew. Chem.* **2010**, *122*, 4114–4128; b) Q. Cao, Y. Li, E. Freisinger, P. Z. Qin, R. K. O. Sigel, Z.-W. Mao, *Inorg. Chem. Front.* **2017**, *4*, 10–32; c) Q. Cao, Y. Li, E. Freisinger, P. Z. Qin, R. K. O. Sigel, Z.-W. Mao, *Inorg. Chem. Front.* **2017**, *4*, 10–32; d) J. Rubio-Magnieto, S. Kajouj, F. Di Meo, M. Fossépré, P. Trouillas, P. Norman, M. Linares, C. Moucheron, M. Surin, *Chem. Eur. J.* **2018**, *24*, 15577–15588; e) J. Rubio-Magnieto, F. Di Meo, M. Lo, C. Delcourt, S. Clément, P. Norman, S. Richeter, M. Linares, M. Surin, *Org. Biomol. Chem.* **2015**, *13*, 2453–2463.
- [24] a) J. E. Reed, S. Neidle, R. Vilar, *Chem. Commun.* **2007**, 4366–4368; b) J. E. Reed, A. J. P. White, S. Neidle, R. Vilar, *Dalton Trans.* **2009**, 2558–2568.
- [25] a) H. Bertrand, D. Monchaud, A. De Cian, R. Guillot, J.-L. Mergny, M.-P. Teulade-Fichou, *Org. Biomol. Chem.* **2007**, *5*, 2555–2559; b) K. Suntharalingam, A. J. P. White, R. Vilar, *Inorg. Chem.* **2009**, *48*, 9427–9435; c) H. Bertrand, S. Bombard, D. Monchaud, E. Talbot, A. Guédin, J.-L. Mergny, R. Grünert, P. J. Bednarski, M.-P. Teulade-Fichou, *Org. Biomol. Chem.* **2009**, *7*, 2864–2871; d) V. S. Stafford, K. Suntharalingam, A. Shivalingam, A. J. P. White, D. J. Mann, R. Vilar, *Dalton Trans.* **2015**, 44, 3686–3700; e) S. Gama, I. Rodrigues, F. Mendes, I. C. Santos, E. Gabano, B. Klejvskaja, J. Gonzalez-Garcia, M. Ravera, R. Vilar, A. Paulo, *J. Inorg. Biochem.* **2016**, *160*, 275–286.
- [26] E. Lary, F. Hamon, F. Rosu, V. Gabelica, E. De Pauw, A. Guédin, J.-L. Mergny, M.-P. Teulade-Fichou, *Chem. Eur. J.* **2011**, *17*, 13274–13283.
- [27] E. Morel, C. Beauvineau, D. Naud-Martin, C. Landras-Guetta, D. Verga, D. Ghosh, S. Achelle, F. Mahuteau-Betzer, S. Bombard, M.-P. Teulade-Fichou, *Molecules* **2019**, *24*, 404.
- [28] P. Wang, C.-H. Leung, D.-L. Ma, S.-C. Yan, C.-M. Che, *Chem. Eur. J.* **2010**, *16*, 6900–6911.
- [29] a) R. Kiltyka, J. Fakhouri, N. Moitessier, H. F. Sleiman, *Chem. Eur. J.* **2008**, *14*, 1145–1154; b) K. J. Castor, J. Mancini, J. Fakhoury, N. Weill, R. Kiltyka, P. Englebienne, N. Avakyan, A. Mittermaier, C. Autexier, N. Moitessier, H. F. Sleiman, *ChemMedChem* **2012**, *7*, 85–94.
- [30] D.-L. Ma, C.-M. Che, S.-C. Yan, *J. Am. Chem. Soc.* **2009**, *131*, 1835–1846.
- [31] Q.-P. Qin, J.-L. Qin, M. Chen, Y.-L. Li, T. Meng, J. Zhou, H. Liang, Z.-F. Chen, *Oncotarget* **2017**, *8*, 61982–61997.
- [32] N. H. Abd Karim, O. Mendoza, A. Shivalingam, A. J. Thompson, S. Ghosh, M. K. Kuimova, R. Vilar, *RSC Adv.* **2014**, *4*, 3355–3363.
- [33] K. Suntharalingam, A. Łęczkowska, M. A. Furrer, Y. Wu, M. K. Kuimova, B. Therrien, A. J. P. White, R. Vilar, *Chem. Eur. J.* **2012**, *18*, 16277–16282.
- [34] a) Z.-F. Chen, Q.-P. Qin, J.-L. Qin, Y.-C. Liu, K.-B. Huang, Y.-L. Li, T. Meng, G.-H. Zhang, Y. Peng, X.-J. Luo, H. Liang, *J. Med. Chem.* **2015**, *58*, 2159–2179; b) Z.-Z. Wei, Q.-P. Qin, T. Meng, C.-X. Deng, H. Liang, Z.-F. Chen, *Eur. J. Med. Chem.* **2018**, *145*, 360–369.
- [35] a) F. Neve, A. Crispini, C. Di Pietro, S. Campagna, *Organometallics* **2002**, *21*, 3511–3518; b) W. Lu, M. C. W. Chan, N. Zhu, C.-M. Che, C. Li, Z. Hui, *J. Am. Chem. Soc.* **2004**, *126*, 7639–7651; c) H.-Q. Liu, T.-C. Cheung, S.-M. Peng, C.-M. Che, *Chem. Commun.* **1995**, 1787–1788.
- [36] S. H. Wadman, J. M. Kroon, K. Bakker, R. W. A. Havenith, G. P. M. van Klink, G. van Koten, *Organometallics* **2010**, *29*, 1569–1579.
- [37] a) C. D. Little, M. M. Nau, D. N. Carney, A. F. Gazdar, J. D. Minna, *Nature* **1983**, *306*, 194–196; b) E. Johnson, D. C. Ihde, R. W. Macuch, A. F. Gazdar, D. N. Carney, H. Oie, E. Rusell, M. M. Nau, J. D. Minna, *J. Clin. Invest.* **1987**, *79*, 1629–1634; c) C. F. Rochlitz, R. Herrmann, E. de Kant, *Oncology* **1996**, *53*, 448–454; d) P. Khaira, C. D. James, M. Lefkay, *Gene* **1998**, *211*, 101–108; e) J. Huang, D. Jiang, T. Zhu, Y. Wang, H. Wang, Q. Wang, L. Tan, H. Zhu, J. Yao, Y. Hou, *Ann. Thorac. Surg.* **2019**, *107*, 436–443.
- [38] M. Toyoshima, H. L. Howie, M. Imakura, R. M. Walsh, J. E. Annis, A. N. Chang, J. Frazier, B. N. Chau, A. Loboda, P. S. Linsley, M. A. Cleary, J. R. Park, C. Grandori, *Proc. Natl. Acad. Sci. USA* **2012**, *109*, 9545–9550.
- [39] J. W. Shay, W. E. Wright, *Nat. Rev. Genet.* **2019**, *20*, 299–309.
- [40] a) K. C. Liu, K. Röder, C. Mayer, S. Adhikari, D. J. Wales, S. Balasubramanian, *J. Am. Chem. Soc.* **2020**, *142*, 8367–8373; b) A. Traczyk, C. W. Liew, D. J. Gill, D. Rhodes, *Nucleic Acids Res.* **2020**, *48*, 4562–4571; c) B. Heddi, V. V. Cheong, H. Martadinata, A. T. Phan, *Proc. Natl. Acad. Sci. USA* **2015**, *112*, 9608–9613.
- [41] A. Basnet, P. Thapa, R. Karki, Y. Na, Y. Jahng, B.-S. Jeong, T. C. Jeong, C.-S. Lee, E.-S. Lee, *Bioorg. Med. Chem.* **2007**, *15*, 4351–4359.
- [42] M. Bianchi, A. Butti, Y. Christidis, J. Perronnet, F. Barzaghi, R. Cesana, A. Nencioni, *Eur. J. Med. Chem.* **1988**, *23*, 45–52.
- [43] a) R. Karki, P. Thapa, M. J. Kang, T. C. Jeong, J. M. Nam, H.-L. Kim, Y. Na, W.-J. Cho, Y. Kwon, E.-S. Lee, *Bioorg. Med. Chem.* **2010**, *18*, 3066–3077; b) H. Kissarwan, A. Kamar, T. Shoker, T. H. Ghaddar, *Dalton Trans.* **2012**, 41, 10643–10651.
- [44] Y. Huang, D. R. Dalton, P. J. Carroll, *J. Org. Chem.* **1997**, *62*, 372–376.
- [45] a) H. Yu, X. Wang, M. Fu, J. Ren, X. Qu, *Nucleic Acids Res.* **2008**, *36*, 5695–5703; b) J. Wang, Y. Chen, J. Ren, C. Zhao, X. Qu, *Nucleic Acids Res.* **2014**, *42*, 3792–3802; c) A. Zhao, S. E. Howson, C. Zhao, J. Ren, P. Scott, C. Wang, X. Qu, *Nucleic Acids Res.* **2017**, *45*, 5026–5035.
- [46] A. J. Phillips, Y. Uto, P. Wipf, M. J. Reno, D. R. Williams, *Org. Lett.* **2000**, *2*, 1165–1168.
- [47] a) D. R. Williams, P. D. Lowder, Y.-G. Gu, D. A. Brooks, *Tetrahedron Lett.* **1997**, *38*, 331–334; b) G. A. Blankson, D. S. Pilch, A. A. Liu, L. F. Liu, J. E. Rice, E. J. LaVoie, *J. Bioorg. Med. Chem.* **2013**, *21*, 4511–4520.
- [48] a) T. Doi, M. Yoshida, K. Shin-ya, T. Takahashi, *Org. Lett.* **2006**, *8*, 4165–4167; b) S. G. Rzuczek, D. S. Pilch, A. Liu, L. Liu, E. J. LaVoie, J. E. Rice, *J. Med. Chem.* **2010**, *53*, 3632–3644; c) F. Hamon, E. Lary, A. Guédin-Beaupaire, M. Rouchon-Dagois, A. Sidibe, D. Monchaud, J.-L. Mergny, J.-F. Riou, C.-H. Nguyen, M.-P. Teulade-Fichou, *Angew. Chem. Int. Ed.* **2011**, *50*, 8745–8749; *Angew. Chem.* **2011**, *123*, 8904–8908; d) M. Petenzi, D. Verga, E. Lary, F. Hamon, F. Doria, M.-P. Teulade-Fichou, A. Guédin, J.-L. Mergny, M. Mella, M. Freccero, *Chem. Eur. J.* **2012**, *18*, 14487–14496; e) N. Rizeq, S. N. Georgiades, *Eur. J. Org. Chem.* **2016**, *2016*, 122–131; f) N. Rizeq, S. N. Georgiades, *Molecules* **2017**, *22*, 2160.
- [49] a) J. Schneider, P. Du, P. Jarosz, T. Lazarides, X. Wang, W. W. Brennessel, R. Eisenberg, *Inorg. Chem.* **2009**, *48*, 4306–4316; b) W. Lu, B.-X. Mi, M. C. W. Chan, Z. Hui, C.-M. Che, N. Zhu, S.-T. Lee, *J. Am. Chem. Soc.* **2004**, *126*, 4958–4971.
- [50] J. V. Gavette, C. M. Klug, L. N. Zakharov, M. P. Shores, M. M. Haley, D. W. Johnson, *Chem. Commun.* **2014**, 50, 7173–7175.
- [51] S. Verma, S. A. Ghuge, V. Ravichandiran, N. Ranjan, *Spectrochim. Acta Part A* **2019**, *212*, 388–385.
- [52] a) J. Dai, M. Carver, L. H. Hurley, D. Yang, *J. Am. Chem. Soc.* **2011**, *133*, 17673–17680; b) A. Gluszyńska, B. Juszkowiak, M. Kuta-Siejkowska, M. Hoffmann, S. Haider, *Int. J. Biol. Macromol.* **2018**, *114*, 479–490.
- [53] a) G. Venkataramana, S. Sankararaman, *Org. Lett.* **2006**, *8*, 2739–2742; b) R. Nandy, M. Subramoni, B. Varghese, S. Sankararaman, *J. Org. Chem.* **2007**, *72*, 938–944.
- [54] S. Bandeira, J. Gonzalez-Garcia, E. Pensa, T. Albrecht, R. Vilar, *Angew. Chem. Int. Ed.* **2018**, *57*, 310–313; *Angew. Chem.* **2018**, *130*, 316–319.
- [55] A. De Cian, L. Guittat, M. Kaiser, B. Sacca, S. Amrane, A. Bourdoncle, P. Alberti, M.-P. Teulade-Fichou, L. Lacroix, J.-L. Mergny, *Methods* **2007**, *42*, 183–195.
- [56] S. Di Fonzo, J. Amato, F. D'Aria, M. Caterino, F. D'Amico, A. Gessini, J. W. Brady, A. Cesaro, B. Pagano, C. Giancola, *Phys. Chem. Chem. Phys.* **2020**, *22*, 8128–8140.
- [57] P. Stadlbauer, M. Krepl, T. E. Cheatham, J. Koča, J. Šponer, *Nucleic Acids Res.* **2013**, *41*, 7128–7143.
- [58] R. Rocca, F. Palazzesi, J. Amato, G. Costa, F. Ortuso, B. Pagano, A. Randazzo, E. Novellino, S. Alcaro, F. Moraca, A. Artese, *Sci. Rep.* **2020**, *10*, 1–11.
- [59] S. P. A. Fodor, R. P. Rava, T. R. Hays, T. G. Spiro, *J. Am. Chem. Soc.* **1985**, *107*, 1520–1529.
- [60] C. Wei, G. Jia, J. Yuan, Z. Feng, C. Li, *Biochemistry* **2006**, *45*, 6681–6691.
- [61] M. Tsuboi, M. Komatsu, J. Hoshi, E. Kawashima, T. Sekine, Y. Ishido, M. P. Russell, J. M. Benevides, G. J. Thomas, *J. Am. Chem. Soc.* **1997**, *119*, 2025–2032.
- [62] L. J. Farrugia, *J. Appl. Crystallogr.* **1999**, *32*, 837–838.

- [63] C. F. Macrae, I. J. Bruno, J. A. Chisholm, P. R. Edgington, P. McCabe, E. Pidcock, L. Rodriguez-Monge, R. Taylor, J. van de Streek, P. A. Wood, *J. Appl. Crystallogr.* **2008**, *41*, 466–470.
- [64] M. D. Hanwell, D. E. Curtis, D. C. Lonie, T. Vandermeersch, E. Zurek, G. R. Hutchison, *J. Cheminf.* **2012**, *4*, 17.
- [65] A. K. Rappe, C. J. Casewit, K. S. Colwell, W. A. Goddard III, W. M. Skiff, *J. Am. Chem. Soc.* **1992**, *114*, 10024–10035.
- [66] A. Ambrus, D. Cheng, J. Dai, R. A. Jones, D. Yang, *Biochemistry* **2005**, *44*, 2048–2058.
- [67] N. M. Hassan, A. A. Alhossary, Y. Mu, C.-K. Kwoh, *Sci. Rep.* **2017**, *7*, 15451.
- [68] O. Trott, A. J. Olson, *J. Comput. Chem.* **2010**, *31*, 455–461.
- [69] M. M. Jaghoori, B. Bleijlevens, S. D. Olabbariaga, *J. Comput.-Aided Mol. Des.* **2016**, *30*, 237–249.

Manuscript received: May 15, 2022
Accepted manuscript online: June 21, 2022
Version of record online: August 1, 2022